

POLITECNICO DI TORINO

Dipartimento di Ingegneria Meccanica e Aerospaziale
Corso di Laurea Magistrale in Ingegneria Aerospaziale

TESI DI LAUREA MAGISTRALE

Fuel cell test rig reconfiguration for a space energy provision system



RELATORE:

Prof. Paolo Maggiore

CANDIDATO:

Alessio Cataudella

CORRELATORE:

Ing. Andrea Emanuele Maria Casini

Marzo 2018

Abstract

This thesis study is part of the partnership between the *ESA* and the *Polytechnic of Turin*, to contribute of the development of the energy production and storage system for a future lunar base. It evaluates the possibility to substitute the conventional battery cycle with the fuel cell and the electrolyzer one, thanks to the hydrogen and oxygen (derived from water) as energy storage mean.

The fuel cell technology is not new in the space field, but the latest technology improvements lead it to be reevaluated for new applications. The main advantages of this equipment compared with batteries are: higher power weight ratio, compatibility and integration with the life support system (e.g. conditioning unit, water management system), less launch mass from earth, and so lower costs thanks to the possibility of using in-situ resources (water from ice and regolith). On the other hand, the fuel cells are more complex and more expensive than batteries.

It is opportune to build a simulation environment before designing and testing the full-scale system, in order to have accurate predictions, even in case of requirements and configurations changes, which are typical of the design loop process. Therefore, it is possible to reduce future full-scale experimental costs.

The main purpose of this study is to assemble a test rig, able to contribute to the development and validation of the lumped parameters simulated environment. In particular, it has been done by recovering an old test bench, upgrading it with a new stack and sub-systems, programming a specific control logic and interface, sensing and collecting data through off-the-shelf components (COTS), editing the hand book and the operation procedures. All this operating in a multidisciplinary working environment.

This thesis assay is intended to describe the work done during the internship period within the *Spaceship EAC* program. The document is divided in four main parts: space exploration scenario focus on lunar mission and Fuel Cell technology, Fuel Cell test rig reconfiguration designed and test, future steps and improvements, and lastly conclusion.

Contents

Contents.....	III
List of Figures.....	V
List of Tables.....	VII
Acronyms.....	VIII
1 Introduction.....	1
1.1 Brief Space exploration excursus.....	1
1.2 Why back to the Moon.....	2
1.3 Preliminary mission scenario.....	3
1.3.1 Lunar base site.....	3
1.3.2 Illumination.....	4
1.3.3 Temperature.....	5
1.3.4 Mission architecture.....	7
1.4 Context.....	7
1.5 Stand-Alone Power System.....	9
1.5.1 Photovoltaic (PV) plant.....	10
1.5.2 Fuel cell plan.....	11
1.5.3 Electrolyzer.....	11
1.5.4 Battery plan.....	11
1.6 Fuel Cell.....	11
1.6.1 Fuel Cell application.....	13
1.6.2 Fuel cell electrochemistry.....	14
1.6.3 Fuel Cell classification.....	22
2 Fuel cell test rig reconfiguration.....	28
2.1 Background.....	28
2.2 Initial project goals.....	28
2.3 Old test rig configuration and new stack.....	30
2.4 First contact with FC test rig.....	31
2.5 Action plan.....	33
2.6 Fluid circuits.....	33
2.6.1 Air circuit.....	33
2.6.2 Cooling system.....	34
2.6.3 Hydrogen circuit.....	35
2.7 Control logic.....	37
2.7.1 Power-on block.....	39

2.7.2 Pre-setting block	40
2.7.3 Loop block	40
2.7.4 Shut down	41
2.8 Net architecture	41
2.8.1 PC	41
2.8.2 Master controller	43
2.8.3 Loop controller	44
2.8.4 Low priority sensors controller	45
2.9 Components characterization	45
2.9.1 H ₂ flow meter	45
2.9.2 H ₂ O flow meter	46
2.9.3 Dual stage valve	48
2.9.4 Air compressor	49
2.9.5 H ₂ O pump	51
2.9.6 Arduino	52
2.9.7 Voltage sensor	53
2.10 Sensors	54
2.11 Actuator supply	58
2.12 Graphic interface communication	58
2.13 Unexpected challenges	60
3 Future steps	63
4 Conclusions	65
Bibliography	67

List of Figures

Figure 1: The Global Exploration Roadmap [2].....	2
Figure 2: Main sites of the lunar South Pole [5]	3
Figure 3: Front view of the solar panel and its effective solar elevation.....	5
Figure 4: Yearly average temperature map of the lunar South Pole from LRO Diviner Lunar Radiometer Experiment.....	6
Figure 5: Yearly maximum temperature map of the lunar South Pole from LRO Diviner Lunar Radiometer Experiment	6
Figure 6: Artist concept of a possible future lunar outpost (credit: ESA/Foster + partners).....	7
Figure 7. Comparison between different power sources for space applications	8
Figure 8 Spaceship EAC interest areas	9
Figure 9. Example of PV-Hydrogen SAPS.	10
Figure 10: Basic principle of the FC electrochemistry [18]	12
Figure 11. FC working principia	13
Figure 12: Edge connection of cells in series [18]	15
Figure 13: Fuel cell stack layout visualizing bipolar plates interposition [18]	16
Figure 14: Single PEM cell construction with width dimensions [18]	17
Figure 15: Low temperature fuel cell polarization curve and its losses (Larminie and Dicks 2003).....	17
Figure 16: Low temperature fuel cell polarization [20]	18
Figure 17: Tafel plots for a slow and a fast reaction [18]	19
Figure 18: Effects of the activation losses on the polarization using the values of 0.01, 1.0, and 100 mAcm ⁻²	20
Figure 19: Effect of crossover current on the polarization curve. [18].	21
Figure 20: Contribution to polarization voltage losses of anode and cathode [22].....	22
Figure 21: Low temperature fuel cell performance [17]	23
Figure 22. New stack (top), old stack (bottom).....	29
Figure 23. FC SimuLink scheme.....	29
Figure 24. LUNA rendering	30
Figure 25. Rover MARVIN.....	30
Figure 26. Old test rig configuration	31
Figure 27. Unsealed stack , arrows indicate the unsealed in/output.....	32
Figure 28. Old electronics	32
Figure 29. Air circuit scheme	33
Figure 32. Cooling circuit scheme.....	34
Figure 33. Preheating test.....	34
Figure 34. Hydrogen circuit scheme.....	35
Figure 35. Provisory assembly side view	36
Figure 36. Provisory assembly up view	36
Figure 37 Flow diagram	37
Figure 38. Sub flow chart	38
Figure 39. Flow chart detail.....	39
Figure 40. Master switch (1) and start operations switch (2).....	40

Figure 41. Net architecture	41
Figure 42. Graphical interface in Vb.NET. Default interface pattern while the program is not running.....	42
Figure 43 Arduino workspace script	44
Figure 44. Differences between the measured and real flow	46
Figure 45. Water flow meter test set-up	47
Figure 46. Coefficient extrapolation graph.....	47
Figure 47. DSV tests experimental scheme.....	48
Figure 48. Experimental setup.....	48
Figure 49. Flow - Pressure characterization curve	49
Figure 50. Air pump characterization.....	49
Figure 51 Original data.....	50
Figure 52 Noise reduced data	50
Figure 53. Water pump test set.....	51
Figure 54. Value comparison	52
Figure 55. Error distribution.....	52
Figure 56. Voltage sensor (45A) characterization chart.....	53
Figure 57. Attempt of current characterization (45 A type).....	54
Figure 58. Sensor circuit.....	55
Figure 59. Futures of the ordered Electric water pump.....	61
Figure 60. Final packaging and storage.....	63

List of Tables

Table 1: Illumination data of the DEM and the solar panel [10].....	5
Table 2: Comparison of FCs used in manned space missions (Halpert at al. 1999)	14
Table 3: Anode ,cathode and cell chemical reactions [18].....	23
Table 4: Comparison between different fuel cell technologies [18].	26
Table 5: Range of power outputs with the different FC technologies available today [18].....	26
Table 6. Features of voltage sensors.....	54
Table 7. Relation wire color - signal	57

Acronyms

FC	Fuel Cell
SAPS	Stand Alone Power System
EAC	European Astronaut Centre
ISECG	International Space Coordination Group
GER	Global Exploration Roadmap
ISS	International Space Station
aDSH	evolvable Deep Space Habitat
ISRU	In Situ Resources Utilization
PV	Photovoltaic
DEM	Digital Elevation Model
ESA	European Space Agency
ECLSS	Environmental Control and Life Support System
BOL	Beginning Of Life
EOL	End Of Life
PEM	Proton Exchange Membrane
DoD	Depth of Discharge
EZ	Electrolyzer
DC	Direct Current
UAV	Unmanned Aerial Vehicles
DSV	Dual Stage Valve
MC	Master Control
I ² C	Inter Integrate Circuit
SDA	Serial Data
SCL	Serial Clock

1 Introduction

This chapter introduce the reader on the lunar exploration, focusing on energy themes and fuel cell topic. Furthermore, the following paragraphs are preparatory for a better comprehension of the core of this thesis: Chapter

2 Fuel cell test rig reconfiguration.

1.1 Brief Space exploration excursus

The realization of the Apollo program, in particular the first human step on the Moon on July 20, 1969, ensued a collective interest in space activities, and it had changed the history in so different way that probably, few years before, only some dreamer would have predicted. However, that first enthusiasm, slowly lessened and the public attention, thus founds, turned away toward others themes. Anyway, the following decades of that epochal event, have not been fruitless at all: space vectors, orbiting stations, satellites, probes and rovers.

“The Vision for Space Exploration” [1] over the next decade, publicized by USA in 2004, announced new interest on the Moon and specific studies on the International Space Station (ISS) as training for Mars exploration .

In 2006, fourteen space agencies (Italian, United Kingdom, France, China, Canada, Australia, Germany, European, Indian, Japanese, Korean, United States, Ukraine and Russian) began a consultation on global interests in space exploration. This unprecedented collaboration become the International Space Coordination Group (ISECG), which aim at the peaceful robotic and human space exploration, within the Solar System. This vision was articulated in "The Global Exploration Strategy: The Framework for Coordination" [4], that was released on May 31, 2007.

The actual international effort to prepare for space exploration missions is reflected by the The Global Exploration Roadmap (GER) [2] reflects a common long-range human exploration strategy that begins with the ISS and continue with missions in the lunar vicinity, to evolve capabilities and technologies needed to go further.

The first lunar human expedition is to take place at the end of 2020s [1]. It will be preceded by a series of robotic missions intended to mitigate the risk respect to manned exploration, mission operations and system reliability.

During this first phase, surface robots will be tele-operated by crew based on the evolvable Deep Space Habitat (eDSH) [3] [4], a support station in cis-lunar space: lunar proximity place, probably in the Lagrange point.

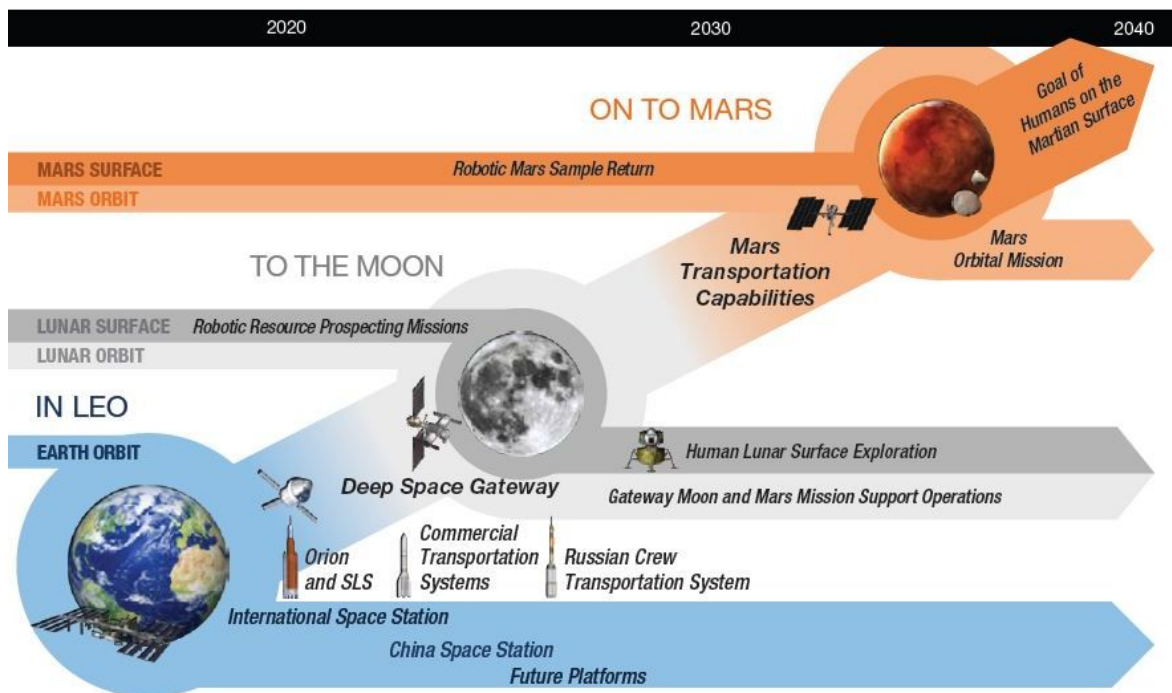


Figure 1: The Global Exploration Roadmap [2]

1.2 Why back to the Moon

A human stable permanence on our satellite would give further consciousness of the birth and evolution of the Earth – Moon system and Solar System as well. While geological processes mutated the Earth (earthquakes, volcanic eruptions, erosions, etc.) the Moon is one of the rare places in the solar system where history has been geologically preserved. The far side of the Moon then, thanks of its radio quietness and the lack of atmosphere, is a great observation point for studying the deep space and the earliest moments of the universe [5]. Finally, the human medicine studies, related to the health adaptation in the hostile environment (radiations, gravity, nutrition etc. etc.).

Lunar exploration will not be motivated only on Mars target: experiences related to In Situ Resources Utilization (ISRU) will be accomplished in extraction and exploitation method of eventual resources such as minerals, oxygen, hydrogen and water, on the lunar south pole,

reducing enormously the Earth dependence. Even, the propellant needed for a hypothetical Mars missions, could be produced on the Moon.

The Moon is thus considered the perfect place to learn the art of planetary surface engineering and operations [5].

1.3 Preliminary mission scenario

There are a lot of possible mission scenarios for a future crewed outpost on the Moon. It is not purpose of this thesis explore all of them, consequently it was chosen as a reference the Carla Careri's study results [5] to have a first idea of the required power plan.

1.3.1 Lunar base site

South polar regions are characterized by several advantages with comparison to the vast majority of lunar surface, from illumination duration to the possible presence of hydrogen and other volatiles. On cons, the landing phase is more challenging. Lunar south pole includes several sites that meet a multi-parameters analysis criterion and satisfy all these requirements, particularly on its high massifs or on the rims of craters.

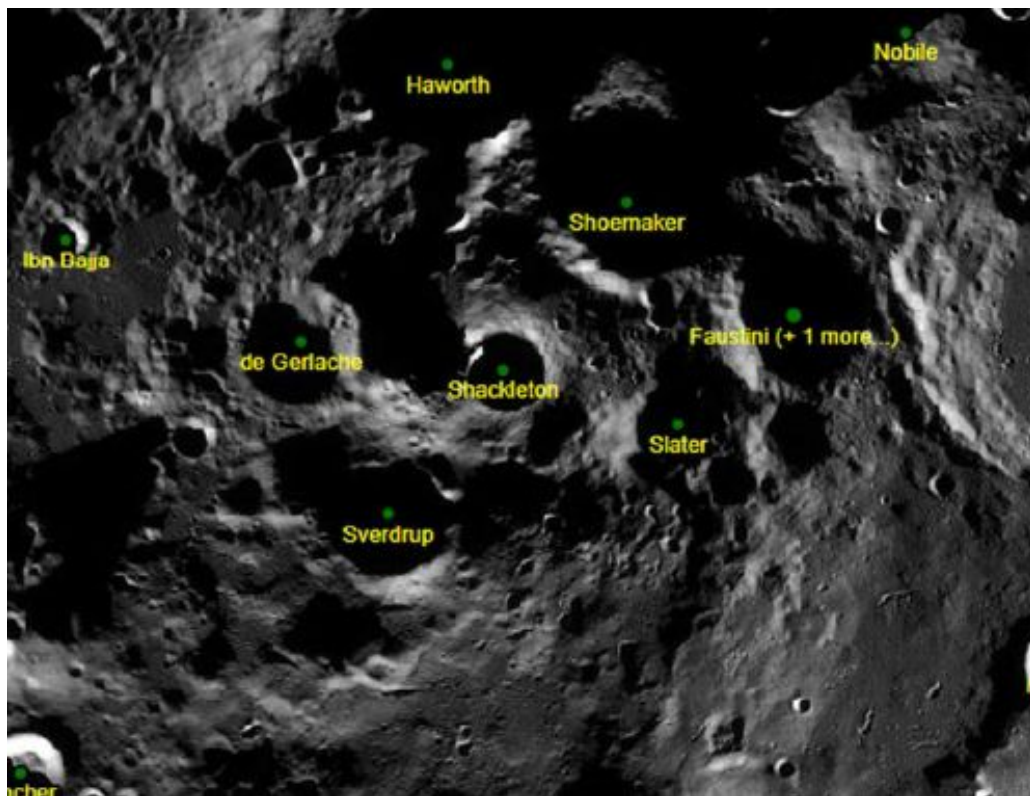


Figure 2: Main sites of the lunar South Pole [5]

The exact landing locations for the foresaw missions still have to be defined, nevertheless, there are different possible sites, and the Shackleton crater's rims could be the elected one for its permanent shadow and extended periods of Sunlight areas. While regions in

permanent shadow may hold ice (called “Cold Traps”) and allow great heat dissipation by heat exchangers, areas receiving nearly constant solar illumination enable almost uninterrupted solar power supply [6]. Finally, the possibility of continuous communication with Earth and the constant visibility of the entire southern sky, which is one the most inviting scientific opportunities related to astronomy [7].

1.3.2 Illumination

The most common data regarding the illumination of a specific area is its average, but it does not describe whether the illumination is distributed in one continuous period or in a large number of short-lasting Sunlit periods. Each of these extremes may produce a very different mass optimum power system design [5].

A typical lunar equator surface is exposed to the Sun for half of the 29.5-day synodic month. For instance, at the lunar equator the average illumination cycle is about 15 days illuminated and 15 days in darkness, a fairly long period for energy storage. The same average illumination value at the poles has much shorter cycles. For this reason, it is essential to have a time varying illumination profile of the candidate deployment site for the power system.

The Moon experiences seasonal insolation variations due to the combined effects of the 5.14° obliquity of the Moon’s orbital plane relative to the ecliptic, and the 6.68° obliquity of the Moon’s spin axis relative to the Moon’s orbital plane [8]. Those combined effects affect the subsolar latitude, which on the Moon currently varies by approximately $\pm 1.54^\circ$ over the course of the Moon’s ~ 346 -days draconic year (shorter than a ~ 365 -days sidereal year), resulting in distinct seasonal insolation and temperature variations [9].

Very little solar direct illumination is actually experienced by the south polar area and the illumination levels are strongly influenced by the effects of topography, as well as the lunar seasons [8]. The Photovoltaic (PV) arrays were designed 2 meter above the surface and vertically installed, to maximize their efficiency [10].

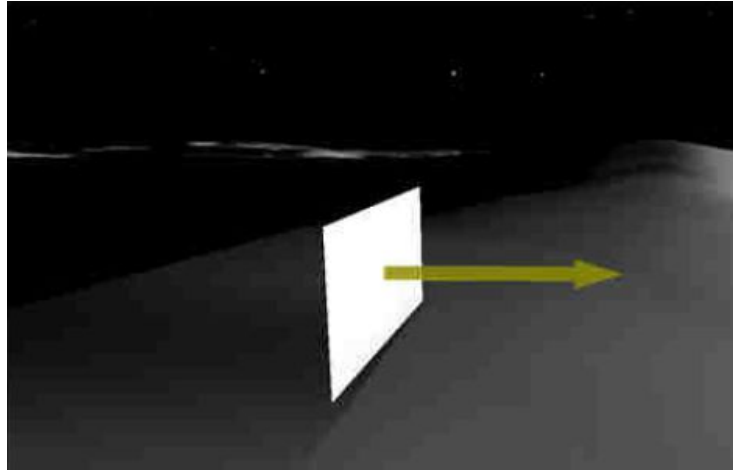


Figure 3: Front view of the solar panel and its effective solar elevation [10]

The illumination data have been calculated from a virtual reality analysis of the panels Digital Elevation Model (DEM). The one year average values are reported in the following *Table 1*.

Longest shadow [days]	Longest sunlit [days]	Eclipse rate [%]	Illumination rate [%]
5.29	126.14	17.12	82.87

Table 1: Illumination data of the DEM and the solar panel [10]

1.3.3 Temperature

With the exception of Mercury, the Moon has the most extreme surface thermal environment of any planetary body in the solar system. The Earth and Moon each receive the same flux of solar radiation; the important difference is that Moon doesn't have atmosphere to insulate its surface [5]. At the equator surface, temperatures show amplitudes of the order of 250K, while the amplitude at the poles is around 100K. Maximum polar temperatures are found to be nearly 170K, while minimum temperatures are around 60K [5].

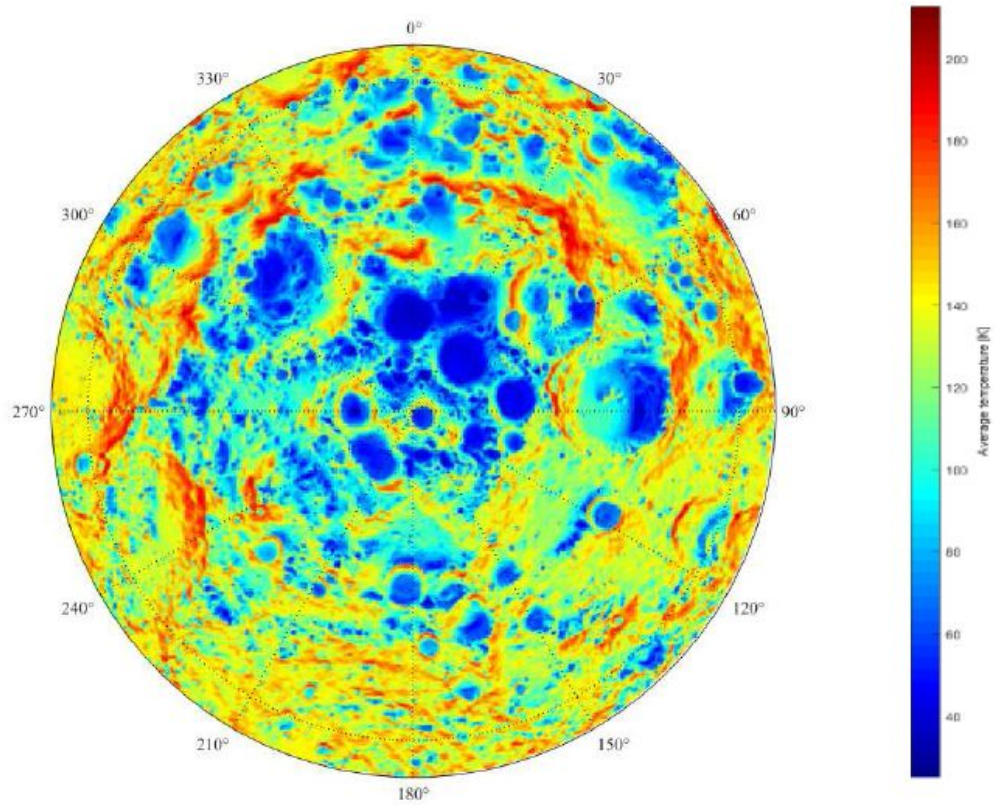


Figure 4: Yearly average temperature map of the lunar South Pole from LRO Diviner Lunar Radiometer Experiment

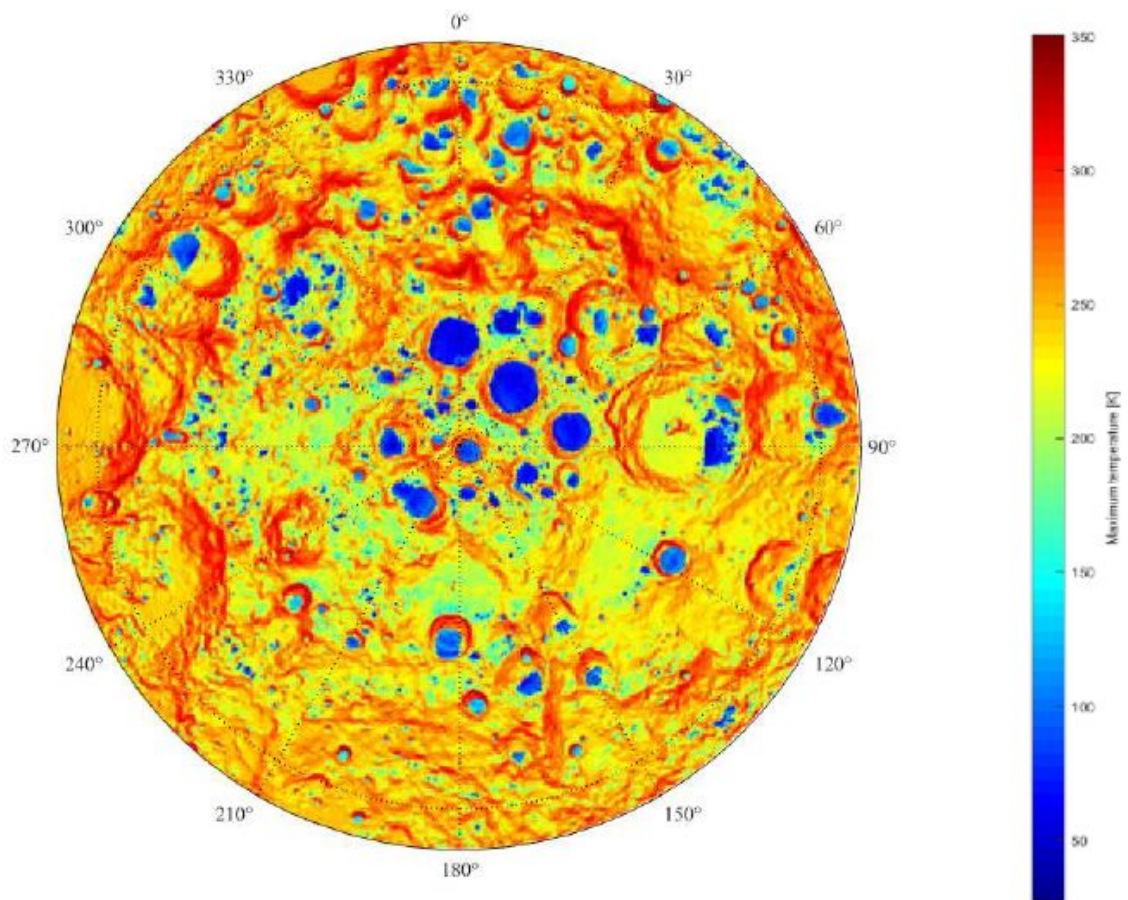


Figure 5: Yearly maximum temperature map of the lunar South Pole from LRO Diviner Lunar Radiometer Experiment

1.3.4 Mission architecture

The main key element to define a mission are: crew number, duration, outpost elements, transportation and power systems. This process has led to consider a permanent outpost where 6 astronauts can operate, such as the ISS. Starting from the ESA artistic impression of the “Moon Village”, an inflatable dome and a rigid pressurized module, double the size of the ISS. Columbus module, have been chose as habitat solution with the same subsystem configuration. Two pressurized rovers and two landers are also present [10]. We are interested on the estimation of absorbs power, therefore, an approximate analysis of the power required by each system has been carried out. Using [11] [12], a preliminary power budget has been derived. The peak power for the base is 887.62 kW, while the housekeeping power (to be maintained during the eclipse period) is 100 kW [10].



Figure 6: Artist concept of a possible future lunar outpost (credit: ESA/Foster + partners)

1.4 Context

Starting from the International Space Station heritage (ISS), a lunar mission could be considered a paramount step for the incremental employment, testing, and validation of new technologies to enable deep space missions. If humans have to reside continuously and productively on the Moon, they must be supported by a lunar infrastructure. For both manned and unmanned mission, energy supply is mandatory and a primary system has to be developed.

An attractive solution is to adopt a photovoltaic-hydrogen Stand Alone Power System (SAPS), using a regenerative FC system in a closed-loop configuration. The main reasons why FC technology is suitable for space applications are the high power densities, if compared to conventional batteries, and a viable alternative to nuclear systems, since it is not yet clarified their usage for human missions due to safety reasons [10].

Another strong point in favour of the SAPS, is its high integration with other systems, such as the Environmental Control and Life Support System (ECLSS). Nevertheless, the design, integration and optimization of each SAPS component is difficult: indeed a robust and adaptable model is desirable.

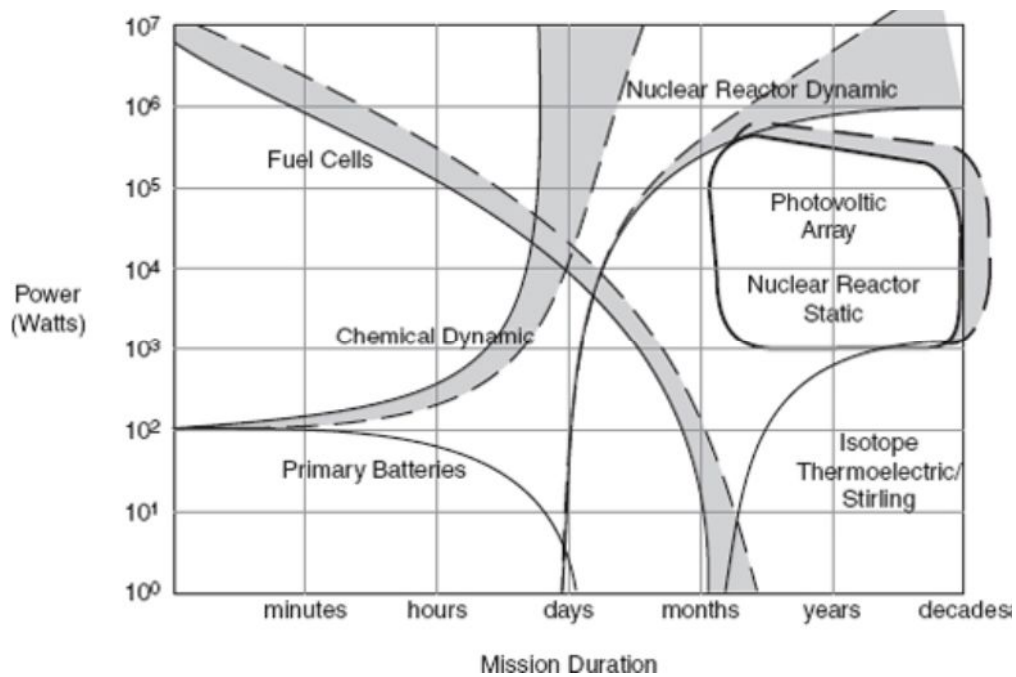


Figure 7. Comparison between different power sources for space applications

As anticipated in the previous chapters, the European Space Agency (ESA) is working on futures lunar missions, in particular since 2012 the European Astronaut Centre (EAC) has found an initiative known as ‘Spaceship EAC’ to investigate innovative technologies and operational concepts in support of ESA’s lunar exploration strategy [13]. The SAPS falls within the Spaceship EAC studied technologies from different points of view, schematize in the following image.

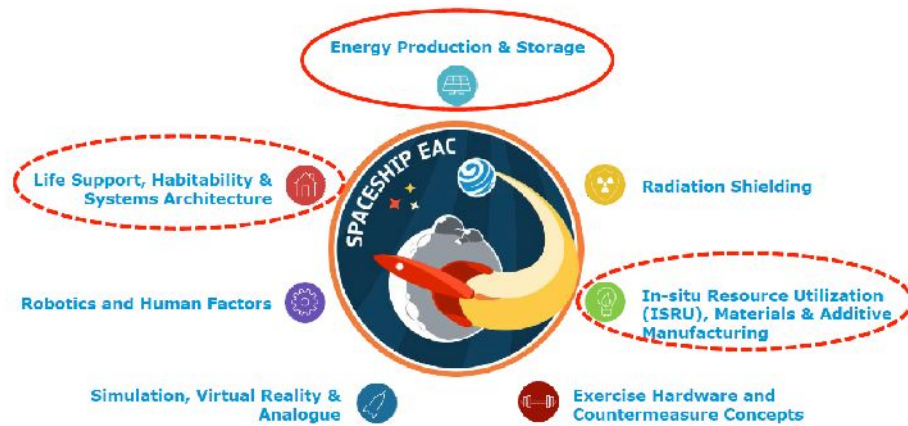


Figure 8 Spaceship EAC interest areas [13]

The main area of interest is *Energy Production & Storage*, for sure, but the SAPS has strictly connections with *Life Support*, because, oxygen and water (as we will see after) are vital for the crew, and can be shared between these systems. Another interaction is with *In-situ Resource Utilization* since icy water is supposed to be present at the lunar poles and could potentially be exploited.

1.5 Stand-Alone Power System

Power required by the outpost, including all the elements previously described, must be supplied by a photovoltaic plant during light periods and by a fuel cell system during eclipse. For redundancy, and to damp power peaks, a high capacity battery system is also included in the mission architecture.

SAPS is defined as an autonomous system which can supply electricity without being connected to the electric grid. Water is the energy carrier and is firstly split through electrolysis in hydrogen and oxygen, and then recombined to obtain energy and again water, in a closed loop scheme.

More precisely, during daylight hours, the sunlight on the photovoltaic arrays is converted into electrical energy, which can be used for electrolysis and for supply power to the lunar infrastructure. The hydrogen and the oxygen produced by the electrolyzer are compressed and stored in tanks. They provide energy for FC, which is design in order to meet the load when the energy produced by the solar arrays is not sufficient.

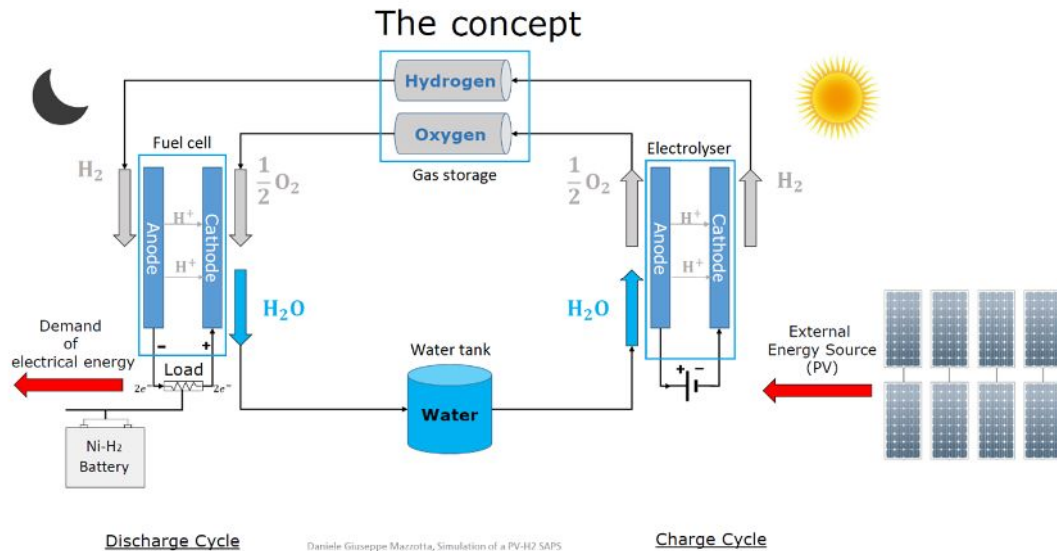


Figure 9. Example of PV-Hydrogen SAPS [10].

Power required can be divided into housekeeping or baseline power, needed continuously, nominal power, which is the average power required in nominal conditions, and peaking power, needed for short periods [5]. Scientific activity or critical tasks, that required high amount of power, can be executed only during t is Sunlit time, thus powered from the photovoltaic plan. As anticipated in the *1.3.4 Mission architecture* paragraph, in order to estimate power plan, ISS data have been used. In specific, since on ISS the housekeeping power is 42.8% of the nominal power (84 kW) [14] [15], the same percentage has been used to compute the lunar outpost housekeeping power modules. The outpost baseline power is then increased by an engineering margin of 13%, giving an output housekeeping power of approximately 100 kW [5].

1.5.1 Photovoltaic (PV) plant

XTJ PRIME space-qualified triple junction solar cells by Spectrolab® have been chosen to meet the peak power requirement. Their Beginning Of Life (BOL) efficiency is 30.7 % [16]. The End Of Life (EOL) calculations has been made assuming 15 years as the maximum expected life before maintenance and replacing operations. A degradation of 0.92 % per year has been assumed from [16]. As a result, the final dimension of the solar panel is 97.55 m wide by 43.70 m high, for a total panel area of 4262.54 m². The sizing led to define the panel architecture as the following:

- 8 power channels, as adopted by the ISS;
- Each channel is composed by 10 arrays connected in parallel;

Each channel will have a nominal voltage of 900 V and a nominal current of 130.74 A [10].

1.5.2 Fuel cell plan

In this mission scenario, the SAPS supplies housekeeping power through two PEM fuel cells stacks. Even if each one fuel cell stack only shall be able to supply 100 kW, it is planned to operate in a hot redundancy configuration at 50 kW each for redundancy and efficiency reasons [5]. Redundancy is underline by the fact that if one of the fuel cells weren't able at a time to provide the base with the required housekeeping power, the crew would take an enormous risk because life support systems could not have power enough to support life [5].

1.5.3 Electrolyzer

The final step that has to be carried out in order to size the SAPS is related to the power required by the electrolyser to produce hydrogen and oxygen starting from the fuel cells waste product: $P_{ez} = 180.24 \text{ kw}$ [5].

1.5.4 Battery plan

In order to improve redundancy, absorbs eventual power peaks demands and respond to emergency conditions, an additional battery plant is included in the power system configuration [5]. The best example of the current state of the art is the Tesla power pack: a battery system that combines lithium-ion batteries, leading electronics, thermal management and controls into a robust and cost-effective turnkey solution. A total of 55 packs would be required to satisfy the power demand, for an overall mass of 89.2 tons, assuming Depth of Discharge DoD = 80% [5].

1.6 Fuel Cell

The fuel cell (FC) is an electrochemical generator, which converts the energy released by a chemical reaction between a fuel (typically hydrogen) and an oxidizer (oxygen) directly into electric energy and heat. FC could be assimilated to a "gas battery" since it converts the chemical energy of a gaseous fuel directly into DC electricity. However, unlike a battery, it does not run out of energy, but can produce electricity as long as fuel is supplied. A typical fuel gas is pure hydrogen or a hydrogen-rich mixture and an oxidant; hydrogen and oxygen are combined to produce electricity, water and heat. The energy conversion is direct from chemical to electrical. Since the process is isothermal, the conversion efficiency is not limited by the Carnot efficiency: a high percentage of the fuel chemical energy is converted directly into electricity skipping the usual combustion step of conventional power systems [17]. FC efficiency, therefore, can be about twice than that of the thermodynamic converters,

achieving values from 65 to 90%, and superior reliability with no moving parts (excluding the auxiliaries).

The basic operating principle of the hydrogen FC is extremely simple.

The first demonstration of a FC was led by the lawyer and scientist William Grove in 1839, where was took advantage from the reverse use of the electrolysis of water. The electrolysis was discover at first as simpler process: electricity passes between two electrodes in water to produce hydrogen and oxygen Figure 10: Basic principle of the FC electrochemistry Figure 10 [18].

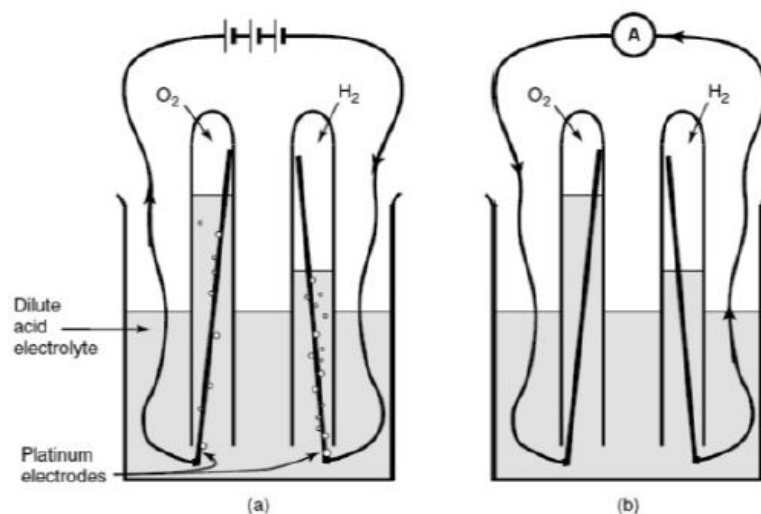


Figure 10: Basic principle of the FC electrochemistry [18]

A FC stack is composed by individual cells connected in series. As a chemical battery, FC is made up of two electrodes, cathode and anode where the reduction and oxidation reactions take place respectively. An electrolyte (both liquid and solid), which allows ions migration, closes the electrical circuit into the cell. Despite of classical batteries, where the fuel is built-in as expendable electrodes, the reactants are continuously renewed, so the cell can give permanent and constant power as output. The hydrogen and the oxidant gas (oxygen or air) arrive respectively to the anode and cathode. Thanks to the porosity of the electrode, the chemical reactions are continuously fed [17].

At the anode (negative pole), hydrogen atoms release electrons (oxidation reaction) and the H^+ ions migrate into the electrolyte; contemporary, the lost electrons move along the anode and enter the external electric circuit. At the cathode (positive pole), oxygen gains the lost hydrogen electrons coming from the external circuit (reduction reaction) and becomes an O_2 ion. At this point, hydrogen ions move towards the cathode where they recombine with O_2 , forming water as waste product [17].

The fuel cell releases heat at the operating temperature too. For an optimum reaction velocity, the operating temperature must be kept in a proper range of values. Therefore, a dedicated temperature control system needs to be added to the cell to maintain a constant temperature [17].

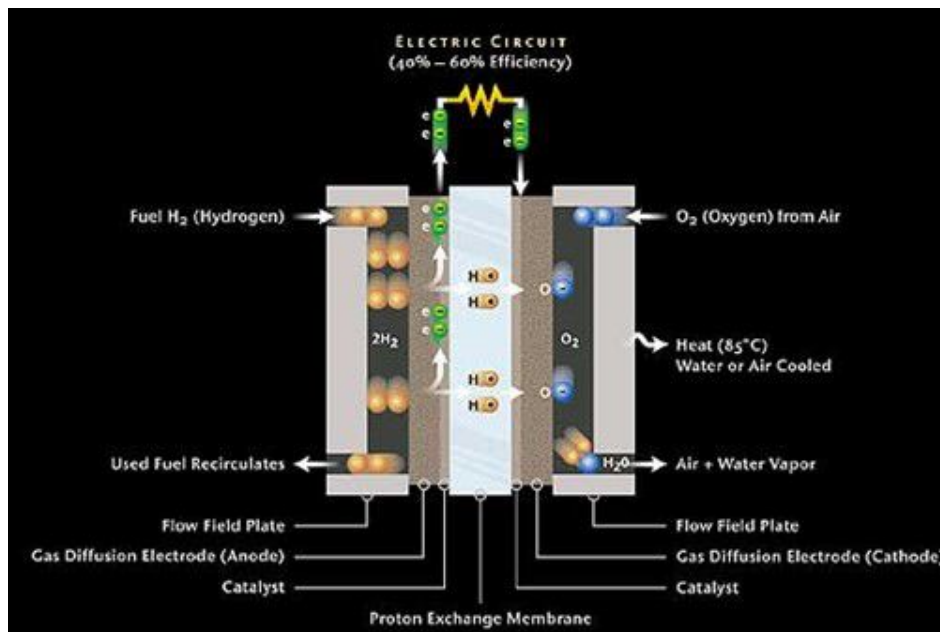


Figure 11. FC working principia [17]

1.6.1 Fuel Cell application

The first use of a FC system in space was in the Gemini program on August 21st, 1962 were was launched with a Proton Exchange Membrane (PEM) electrolyte fuel cell known at that time as the solid polymer electrolyte ion exchange membrane fuel cell [17].

The Biosatellite 2, launched September 7, 1967, utilized a PEM fuel cell system with an important change involving the use of an improved membrane material known as Nafion® (a sulfonated tetrafluorethylene e copolymer), a registered trademark of the DuPont Company [17].

Subsequent Apollo manned flights (1968-72) utilized the alkaline electrolyte fuel cell containing potassium hydroxide electrolyte held in an asbestos separator. The shuttle orbiter fuel cell power plant contained three H₂/O₂ alkaline fuel cell power plants supplying 12 kW at peak and 6 kW of average power. The system was capable of 2,000 hours of operation. The shuttle orbiter fuel cell power plant was 23 kg lighter and delivered eight times the power of the Apollo fuel cell system *Table 2* [17].

Characteristic	Mission		
	Gemini	Apollo	Space Shuttle
Stack type / units	PEM / 3	AFC / 2	AFC / 3
Energy (kWh/unit)	65	115	2600
Current density ($mAcm^{-2}$)	36	68	172
Average power (W/unit)	1000	1420	7000
Stack specific power (Wkg^{-1})	33.33	12.99	60.87
Stack mass (kg)	30	110	115
Lifetime (h)	1000	400	2000

Table 2: Comparison of FCs used in manned space missions (Halpert et al. 1999)

In the aeronautics, fuel cells are used for a main propulsion supplier and/or auxiliary power generator. In the first application the FC provides electric energy to one or more electric motors (in substitution of a conventional internal combustion engine) driving the propeller for small airplanes (e.g. general aviation class), Unmanned Aerial Vehicles (UAVs) or gliders. In this case, the FC sully absolve the second application too: provides all of the electric energy required by on-board equipment (avionics and electronics), making the vehicle “all electric”. PEM fuel cells are currently adopted for this purpose.

Auxiliary Power Units (APUs) and Ground Power Units (GPUs) falling as the second aeronautical type application. In this case the FC converts chemical energy to electric one, driving pneumatic pumps or gears, in substitution of a conventional oil powered turbine. The SOFC and the PEM technologies are usually adopted.

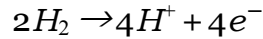
Can be interested reported the FC integration in civil applications on Earth as night power supply. The working principia is the same of the *1.5 Stand-Alone Power System*, providing energy to buildings in a completely autonomous way. An example is the “housing of grid” of the “Phi Suea House” project on Thailand [19].

1.6.2 Fuel cell electrochemistry

It is convenient to consider the separate reactions taking place at each electrode to explain the formation of water from hydrogen and oxygen, and how the flow of electrons (current) is generated.

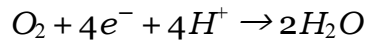
Considering a PEM fuel cell, at the anode the hydrogen gas is ionized when enter in contact with the catalyser on the membranes, releasing electrons that collected from the electrode

(anode) and creating H^+ ions (protons) which flow through the membrane toward the cathode:



The electrons constitute the current that circulates in the external electric circuit powering the load, thus releasing part of their energy.

At the cathode, oxygen reacts with electrons coming from the electrode, and H^+ ions from the electrolyte in the membrane, to form water:



For both these reactions proceed continuously as long as the reactants are provided and temperature and load are inside the working range. Certain polymers can also transfer the mobile H^+ ions. These materials are called proton exchange membranes (PEM). The electrolyte must only allow H^+ ions to pass through it, and not electrons; otherwise, the electrons would go through the electrolyte, losing all of the electric current produced. Clearly, the entire process is exoenergetic since the formation enthalpy of the H_2 and O_2 is major than water molecule: the energy produced (chemical) is transform in thermal and electric energy.

The voltage of a fuel cell is quite small, about 0.7 V. This means that to produce a useful voltage many cells have to be connected in series. Such a collection of fuel cells in series is known as a "stack" The most obvious way to do this is by simply connecting the edge of each anode to the cathode of the next cell, as in Figure 12: Edge connection of cells in series [17].

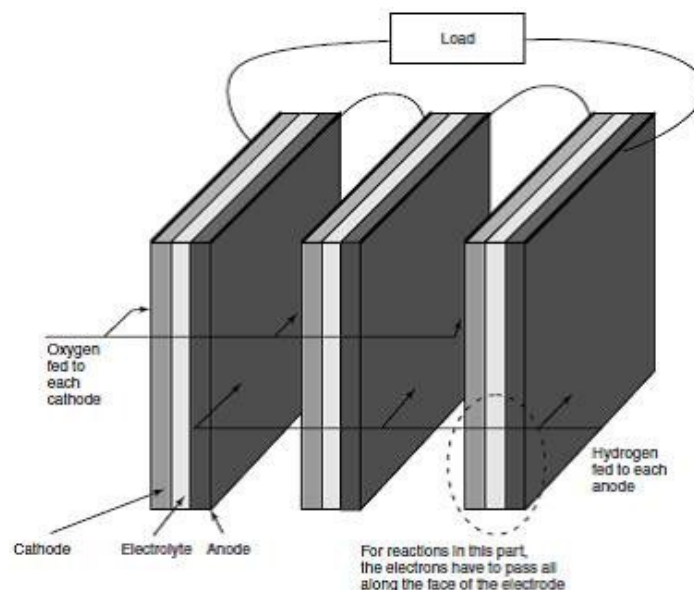


Figure 12: Edge connection of cells in series [18]

The problem with this method is that the electrons have to flow across the face of the electrode to the current collection point at the edge. The electrodes might be quite good conductors, but if each cell is only operating at about 0.7 V, even a small voltage drop is important. A much better method of cell interconnection is to use a “bipolar plat”. This makes connections all over the surface of one cathode and the anode of the next cell (hence bipolar); at the same time, the bipolar plate serves as a means of feeding oxygen to the cathode and fuel gas to the anode. Although a good electrical connection must be made between the two electrodes, the two gas supplies must be strictly separated **Figure 13: Fuel cell stack layout visualizing bipolar plates interposition** *Figure 13* [17].

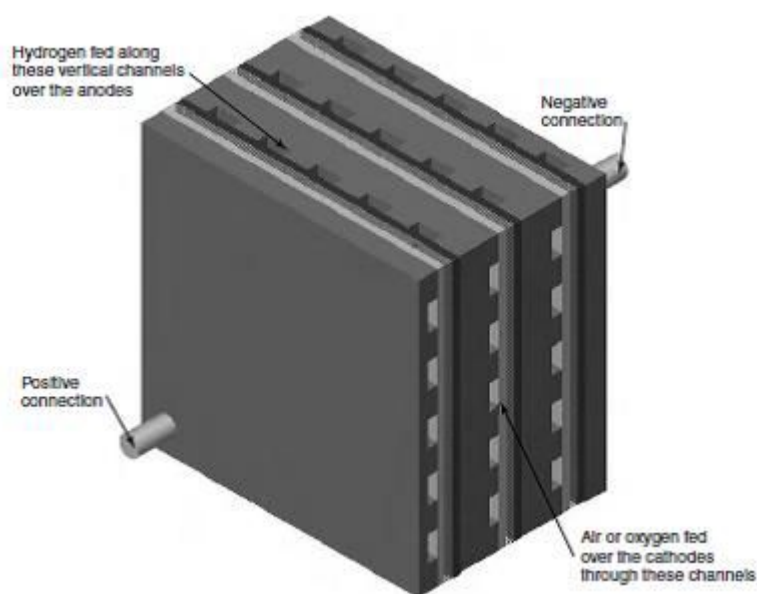


Figure 13: Fuel cell stack layout visualizing bipolar plates interposition [18]

PEFC stacks are almost universally of the planar bipolar type. The polytetrafluoroethylene, or PTFE, also sold as Teflon, has been very important in the development of fuel cells. The strong bonds between the fluorine and the carbon make it durable and resistant to chemical attack. Another important property is that it is strongly hydrophobic, and so it is used in fuel cell electrodes to drive the product water out of the electrode, preventing flooding. More over the basic PTFE polymer is “sulphonated” creating the bases for Nafion® material. A key property of sulphonic acid is that it is highly hydrophilic: it attracts water [17].

The hydrophilic regions around the clusters of sulphonated side chains can lead to the absorption of large quantities of water, increasing the dry weight of the material by up to 50%. The resulting material has different phases – dilute acid regions within a tough and strong hydrophobic structure. Although the hydrated regions are somewhat separate, it is still possible for the H⁺ ions to move through the supporting long molecule structure.

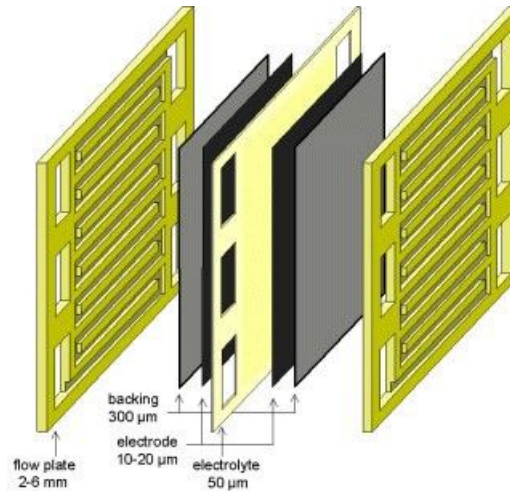


Figure 14: Single PEM cell construction with width dimensions [18]

In fuel cells, several energy losses in form of voltage losses occur, due to several electrical and electrochemical phenomena. The four main losses are: activation losses, exchange current losses, ohmic losses and concentration losses. The following discussion applies for both alkaline and PEM devices. *Figure 15* shows a typical low temperature hydrogen-oxygen fuel cell polarization curve (in black colour) [17]. Four main detrimental effects on the cell voltage are briefly described.

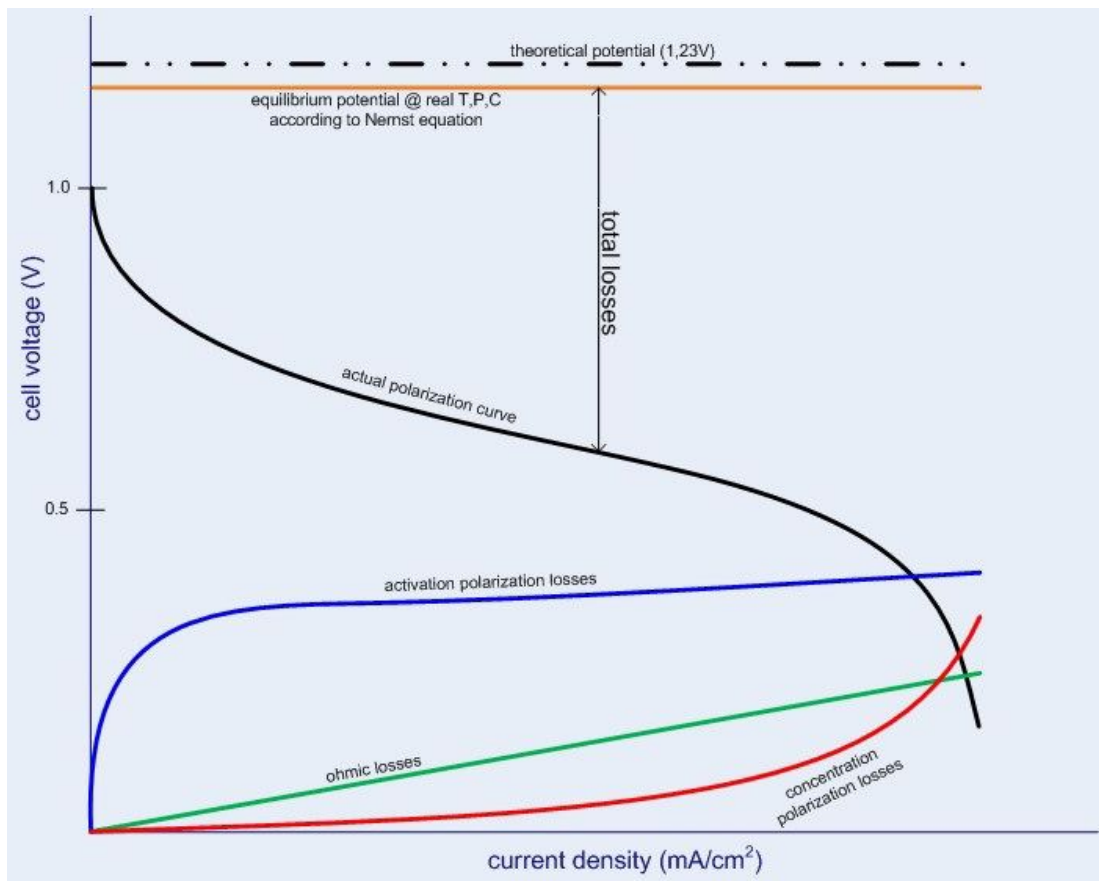


Figure 15: Low temperature fuel cell polarization curve and its losses (Larminie and Dicks 2003)

The *Figure 16* underline which loss is dominant respect the other, in each part of the polarization curve.

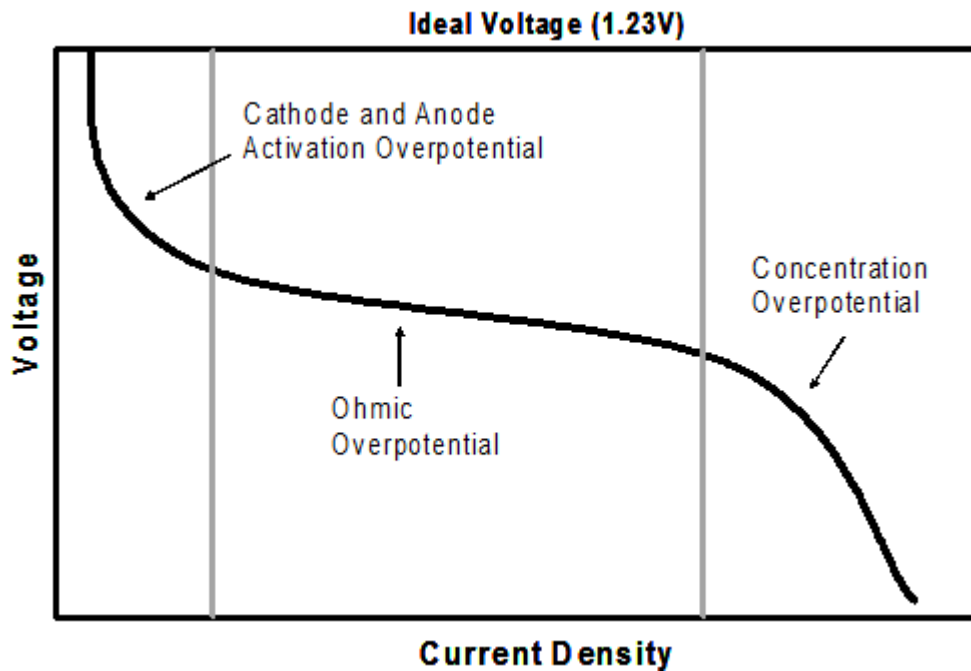


Figure 16: Low temperature fuel cell polarization [20]

Activation losses

Tafel observed and reported in 1905 that the overvoltage at the surface of an electrode followed a similar pattern reported in *Figure 17* known as Tafel plots. It shows the overvoltage (i.e. voltage loss, V) against the logarithm of current density. For most values of overvoltage, the graph approximates them to a straight line [18]. Although the Tafel equation was originally deduced from experimental results, it also has a theoretical basis.

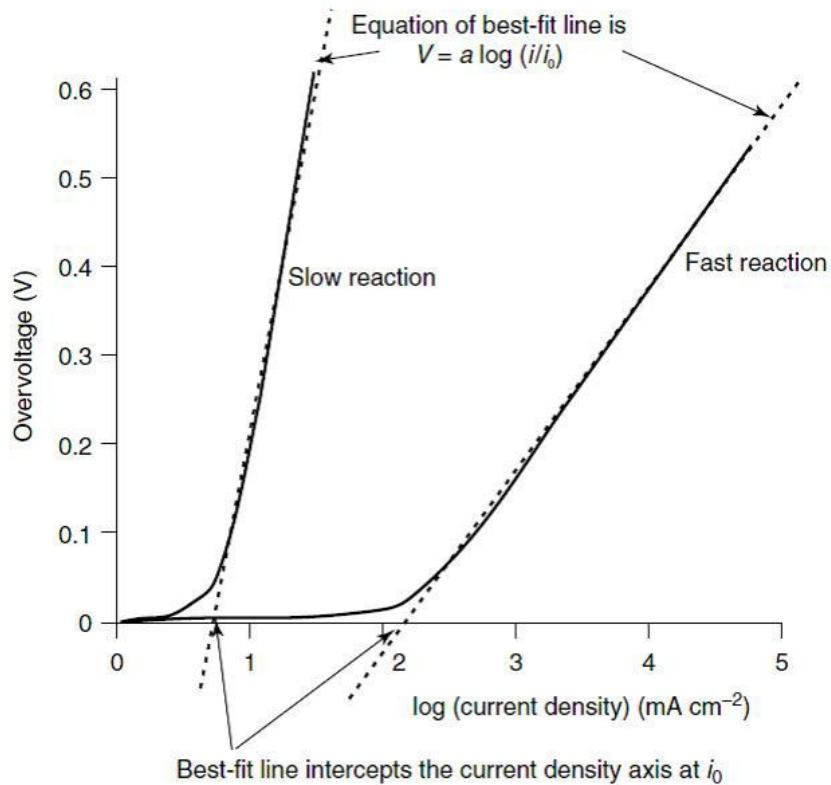
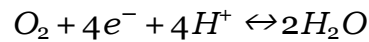


Figure 17: Tafel plots for a slow and a fast reaction [18]

The reaction at the cathode of a PEM FC at zero current density in equilibrium condition is expressed as:



Therefore, there is a continual backwards and forwards flow of electrons from and to the electrolyte, never exiting the cell. This current density is i_0 , the “exchange” current density. It is reasonable to think that if this current density is high, then the surface of the electrode is more “active” or “ready”. In an active electrode, when the current moves in one particular direction is more likely to flow through the electric circuit, simply shifting in one particular direction of a reaction already going on, rather than starting from zero [18]. The exchange current density should be as high as possible to have good FC performance.

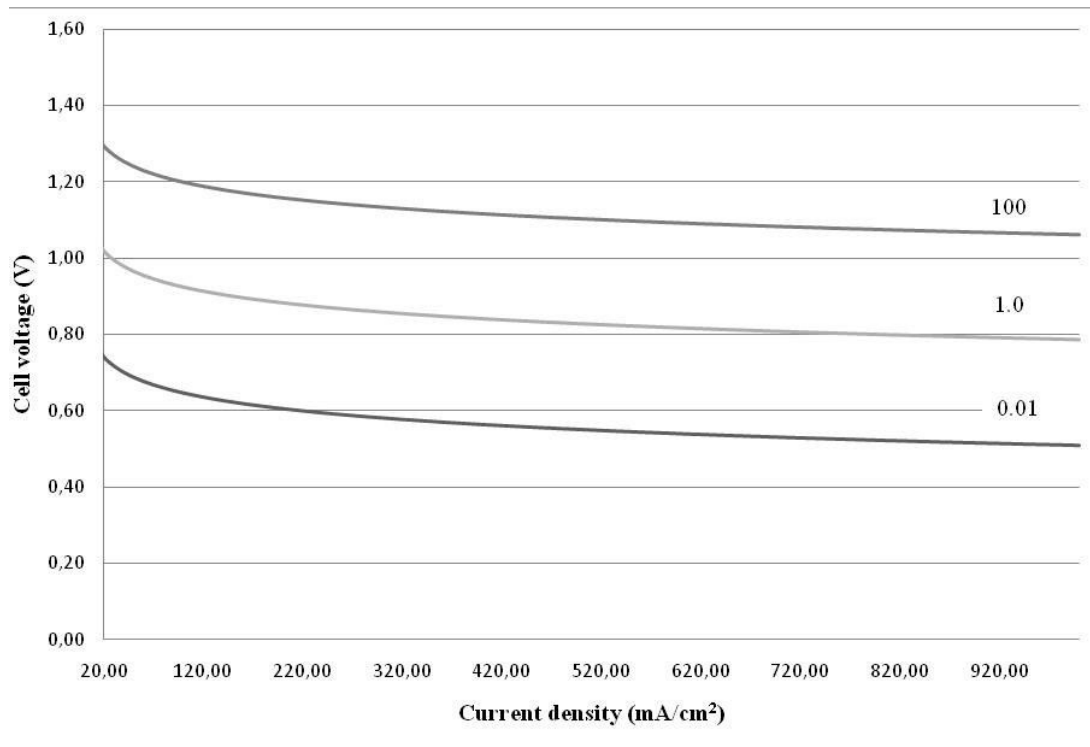


Figure 18: Effects of the activation losses on the polarization using the values of 0.01, 1.0, and 100 mA/cm² for the exchange current density [21] [18].

Crossover currents

An important aspect to be underlined is the fact is that it is possible to recognize that the ideal fuel cell voltage of about 1.23 V at standard conditions, stated theoretically, is never reached at zero current density, as can be seen in *Figure 15*. Although the electrolyte of a fuel cell must be chosen for its proton selective conducting properties, it will always be able to support very small amounts of electron conduction (known as internal currents). However, probably more important in a practical fuel cell is that some hydrogen will diffuse from the anode through the electrolyte to the cathode. Here, because of the catalyst, it will react directly with the oxygen, producing no current from the cell. This small amount of wasted fuel migrating through the electrolyte is known as fuel crossover [17]. The low temperature FC are more affected from this phenomenon.

A small change in fuel crossover and/or internal current caused, for example, by a change in humidity of the electrolyte, can cause a large change in the open circuit voltage. The equivalence of the fuel crossover and the internal currents on the open circuits is an approximation, but is quite a fair one in the case of hydrogen fuel cells where the cathode activation overvoltage dominates [17].

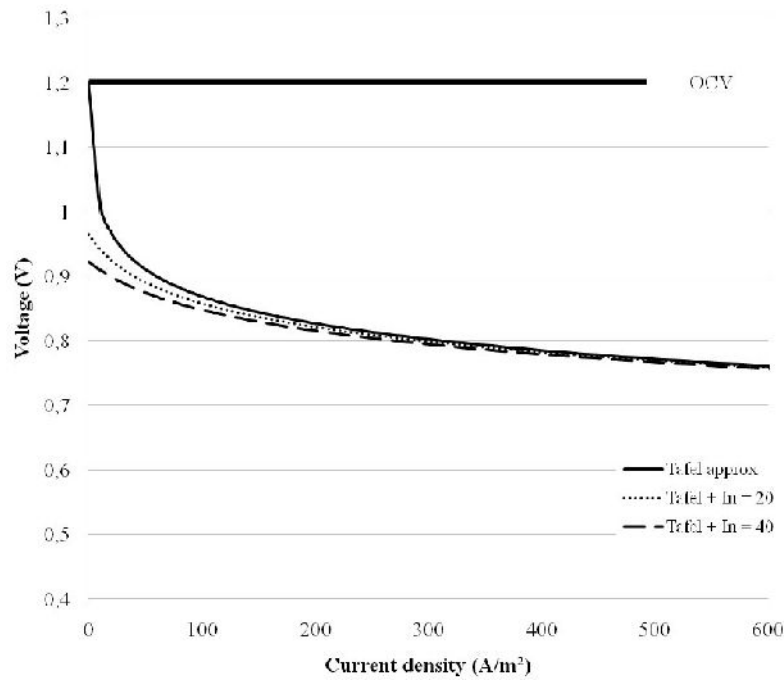


Figure 19: Effect of crossover current on the polarization curve. [18].

Ohmic losses

The electrical resistance of the electrodes, and the resistance to the flow of ions in the electrolyte, are the main responsible of the ohmic losses. The electrolyte (membrane in case of PEM or similar cells) is usually the main cause, since the cell plates and gas diffusion layers and current collectors are highly conductive media.

A mitigation can be achieved with the use of electrodes with the highest possible conductivity and making the electrolyte as thin as possible. It also must be thick enough to prevent any shorting of one electrode to another through the electrolyte, which requires a certain level of physical robustness [17].

Figure 20 plots the voltage losses contributing to a decrease in the open-circuit voltage. As can be seen, cathode activation losses (cathode loss, fed with air or pure oxygen) are the main form of voltage drop, followed by ohmic losses (indicated as Electrolyte IR Loss); the anode activation loss (Anode Loss) is quite negligible [17].

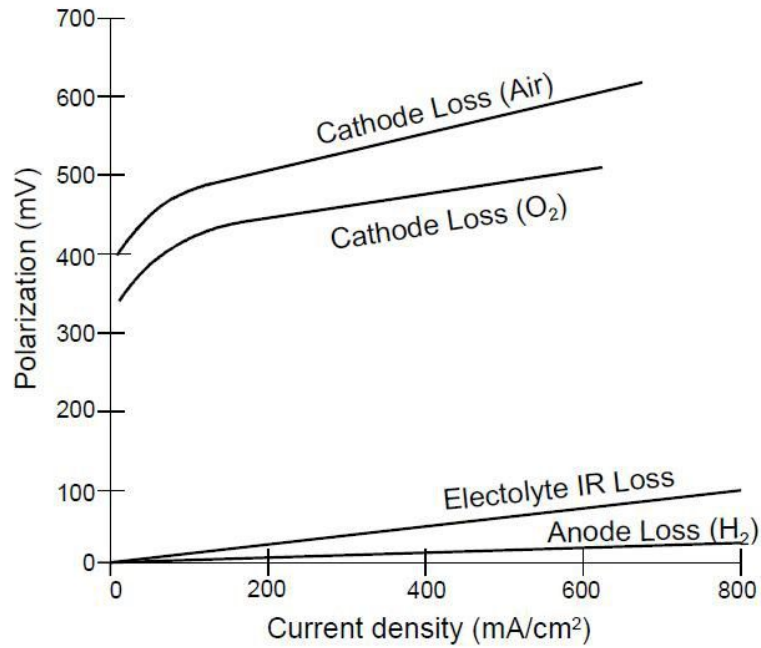


Figure 20: Contribution to polarization voltage losses of anode and cathode [22]

Concentration losses

As a reactant is consumed at the electrode by electrochemical reactions, it is often diluted by the products, since finite mass transport rates limit the supply of fresh reactant and the evacuation of products. Consequently, a concentration gradient is formed between the reactive surface and the fluid flow inside the channel, driving the mass transport process [17]. In a cell with purely gas phase reactants and products, gas diffusion processes control mass transfer. In other cells, multi-phase flow in the porous electrodes can have a significant impact. In fuel cells, the evacuation of product is often more limiting than the supply of fuel, given the difference between the diffusivity of hydrogen and water (vapour). For electrolyzers using submerged electrodes, concentration losses are not a particular issue, since it would be sufficient to remove the produced gases from the electrode surface to allow water to reach the reaction sites [17].

1.6.3 Fuel Cell classification

Different fuel cell classifications are available. One of the main and at high level subdivision based of FC operating temperature, which is coupling with different fuels used: low-temperature and high-temperature FC.

Fuel cell technology	Anode reaction	Cathode reaction	Cell reaction
Low temperature fuel cells			
Solid polymer	$H_2 \rightarrow 2H^+ + 2e^-$	$\frac{1}{2} O_2 + 2H^+ + 2e^- \rightarrow H_2O$	$H_2 + \frac{1}{2}O_2 \rightarrow H_2O$
Phosphoric acid	$H_2 \rightarrow 2H^+ + 2e^-$	$\frac{1}{2} O_2 + 2H^+ + 2e^- \rightarrow H_2O$	$H_2 + \frac{1}{2}O_2 \rightarrow H_2O$
Alkaline	$H_2 + 2(OH)^- \rightarrow 2H_2O + 2e^-$	$\frac{1}{2}O_2 + H_2O + 2e^- \rightarrow 2(OH)^-$	$H_2 + \frac{1}{2}O_2 \rightarrow H_2O$
Peroxide	$NaBH_4 + 8Na^+ + 8(OH)^- \rightarrow NaBO_2 + 6H_2O + 8Na^+ + 8e^-$	$8Na^+ + 8e^- + 4H_2O_2 \rightarrow 8Na^+ + 8(OH)^-$	$NaBH_4 + 4H_2O_2 \rightarrow NaBO_2 + 6H_2O$
High temperature fuel cells			
Solid oxide	$H_2 + O^{2-} \rightarrow H_2O + 2e^-$	$\frac{1}{2} O_2 + 2e^- \rightarrow O^{2-}$	$H_2 + \frac{1}{2}O_2 \rightarrow H_2O$
Molten carbonate	$H_2 + CO_3^{2-} \rightarrow H_2O + CO_2 + 2e^-$	$\frac{1}{2} O_2 + CO_2 + 2e^- \rightarrow CO_3^{2-}$	$H_2 + \frac{1}{2}O_2 \rightarrow H_2O$

Table 3: Anode ,cathode and cell chemical reactions [18]

Low temperature fuel cells

The low temperature fuel cells usually makes use of pure hydrogen as fuel and air or oxygen as oxidant. Most of them operate at temperatures between ambient temperature and 100-150 °C. The electrode is made of a porous material to augment the surface exposed to the hydrogen or oxygen [17].

The following graph (Figure 21) compares four types of FCs : AFC, PEM, H₂/H₂O₂ and NaBH₄/H₂O₂. It results that the better solution is the last one, giving higher current densities and output voltage .

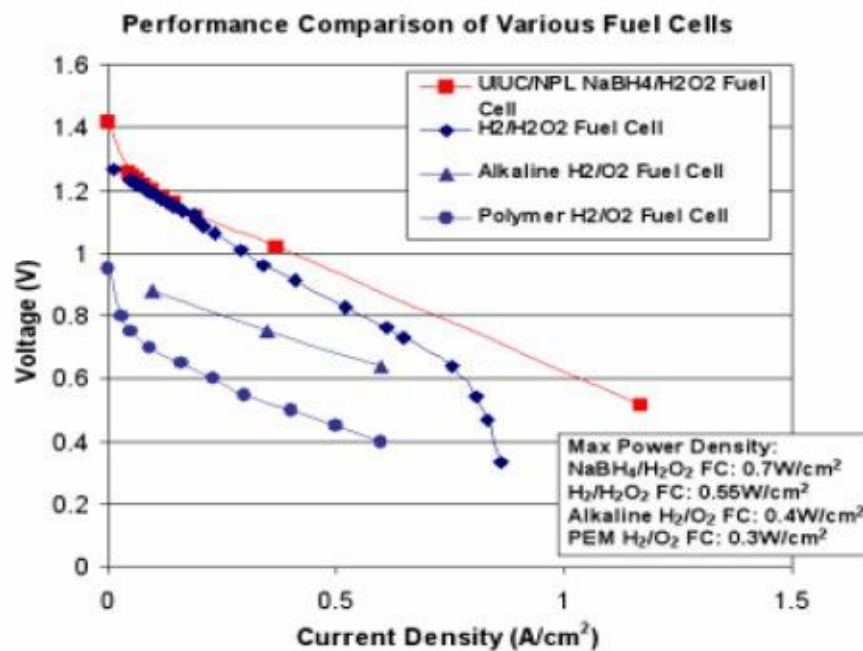


Figure 21: Low temperature fuel cell performance [17]

Alkaline FC (AFC)

Alkaline fuel cells were one of the first fuel cell technologies developed, and they were the first type used in the U.S. space program to produce electrical energy and water onboard spacecraft. Nowadays, an AFC power system can give a 5-80 kW class of power output. These fuel cells use a solution of potassium hydroxide (KOH) in water as the electrolyte and can use a variety of precious or non-precious metals as a catalyst at the anode and cathode (Pt/Ni). High-temperature AFCs operate at temperatures between 100°C and 250°C. However, more-recent AFC designs operate at lower temperatures of roughly 23°C to 70°C. AFCs are high performance fuel cells due to the rate at which chemical reactions take place in the cell. They are also very efficient, reaching efficacies of 60 % in space applications. The disadvantage of this fuel cell type is its easy carbon dioxide(CO₂) poisoning. Moreover, the electrolyte has to circulate through the cell, so the cell needs a KOH circulation circuit. AFC stacks have been shown to maintain sufficiently stable operation for more than 8000 operating hours. Low operating temperatures allow the use of lightweight and inexpensive materials such as graphite and polymers; also, the start-up time is really low, in the order of some minutes [17].

Proton Exchange Membrane FC (PEM, PEFC, SPFC)

Proton Exchange Membrane FC, also called Polymer Electrolyte or Solid Polymer, has low weight and volume, therefore a high power density, compared to other FC type. PEM FC thanks to its fast start-up time (few minutes), low sensitivity to orientation, and good power-to-weight ratio, its application is also extended to land vehicles (i.e. cars) and stationary (buildings). This cell is the best candidate chosen to substitute the old AFCs in space applications. PEM fuel cells use a thin solid polymer (Nafion®) as electrolyte and porous carbon electrodes containing a platinum catalyst, without any corrosive fluids like some FCs. The membrane is sensitive to the humidity, which has to be maintained inside a certain range; furthermore, it must be kept humid even when the FC is inactive. Low temperature operation (around 80°C) allows them to result in less wear on system components, resulting in better durability. The efficiency of these cells is between 50 and 60%. As well as in the case of the AFCs, platinum catalyst is extremely sensitive to CO poisoning. Developers are currently exploring platinum/ruthenium catalysts that are more resistant to CO. The power output could be raised up to 250 kW with the available technology [17].

Phosphoric Acid FC (PAFC)

PAFCs generate electricity from 40% to nearly 85% of efficiency if the out steam is used for cogeneration. These cells use liquid phosphoric acid as the electrolyte and operate at about 200 °C therefore they need a start-up times up to few hours. The medium temperature increases. Even if it is a mature technology for terrestrial applications, they have never been used in space [17].

H₂O₂ based FC

H₂O₂ fuel cells are standard PEM cells, but the typical gaseous pure oxygen that feeds the reaction is substituted by liquid hydrogen peroxide (H₂O₂), thus giving an H₂/H₂O₂ FC. Even the fuel can be replaced by NaBH₄ (sodium tetrahydroborate), a powder which can be dissolved in water or in alkaline solution to be used as fuel, thus creating a NaBH₄/H₂O₂ FC. It is very important to underline that in both cases, the chemical reactions are invertible, and so it is possible to develop a regenerative fuel cell (explained below). The main advantage of this FC type is the reactants storage condition. The fuel and oxidant are liquid at room temperature, consequently, they do not need cryogenic and high pressure tanks; moreover, there is not the problem of the “boiling off” resulting from long-time storage periods. The efficiency (max 80%) and cell voltage are greater than a usual H₂/O₂ based system [17].

High temperature fuel cells

High temperature FCs (up to 1000°C) have the advantage of very high power output and good efficiency (around 60%) which increases up to 85% when coupled with co-generation using the large amount of waste heat to produce electrical energy. This high temperature is feasible for terrestrial stationary applications, nonetheless a big issue for space environment. The chemical reactions occur spontaneously due to the high temperature, so the electrodes do not require the use of Pt as catalyst, and they are not poisoned by carbon monoxide and dioxide (CO, CO₂). On the other hand, the warm-up activation periods is long (order of some hours), and they suffer of fast material degradation which imposes stringent durability requirements on materials [17].

Solid Oxide FC (SOFC)

Solid oxide fuel cells use a hard, non-porous ceramic compound as the electrolyte (zirconium oxide). The high temperature allows SOFCs to reform fuels internally, which enables the use of a variety of fuels [17].

Molten Carbonate FC (MCFC)

Molten carbonate fuel cells are currently being developed for natural gas and coal-based power plants for electrical utility, industrial, and military applications. MCFCs use an electrolyte composed of a molten carbonate salt mixture suspended in a porous, chemically inert ceramic lithium aluminium oxide (LiAlO₂) matrix [17].

Protonic Ceramic FC (PCFC)

This new type of fuel cell is based on a ceramic electrolyte material that exhibits high protonic conductivity at elevated temperatures. PCFCs share the thermal and kinetic advantages of high temperature operation at 700 °C with MCFCs and SOFCs, while exhibiting all of the intrinsic benefits of proton conduction in PEM and PAFC cells. The high operating temperature is necessary to achieve very high electrical fuel efficiency with hydrocarbon fuels. PCFCs can operate at high temperatures and electrochemically oxidize fossil fuels directly to the anode, with carbon dioxide as the primary reaction product [17].

Characteristics	Fuel cell technology				
	AFC	PEM	PAFC	MCFC	SOFC
Electrolyte	KOH	Polymer	Phosphoric acid	Li/Al carbonate	Solid oxide
Temperature (°C)	90 - 100	50 - 100	150 - 200	600 - 700	650 - 1000
Catalyzer	Pt/Pd, Ni	Pt	Pt	Ni	Not needed
Materials	Polymers, graphite, Inconel	Graphite, metals, asbestos	Graphite	Nickel, stainless steel	Ceramics, metals
Efficiency (%)	60 - 70 (electric)	50 - 60 (electric)	80 - 85 (CHP) - 42 (elec)	85 (CHP) 60 (elec)	85 (CHP) 30-60 (elec)
Pow. (mWcm ⁻²)	300 - 500	300 - 900	150 - 300	150	150 - 270
Power (kW)	5 - 80	<1 - 250	50 - 1000	<1 - 1000	5 - 3000
Start-up time	Minutes	Minutes	1 - 4 hrs	5 - 10 hrs	5 - 10 hrs

Table 4: Comparison between different fuel cell technologies [18].

Fuel cell technology	Power (kW)							
	1x10 ⁻³	1x10 ⁻²	1x10 ⁻¹	1	10	100	1,000	10,000
AFC	NO	NO	NO	YES	YES	YES	NO	NO
PEM	YES	YES	YES	YES	YES	YES	NO	NO
PAFC	NO	NO	NO	NO	NO	YES	YES	YES
SOFC	NO	YES	YES	YES	YES	YES	YES	YES
MCFC	NO	NO	NO	NO	NO	YES	YES	NO

Table 5: Range of power outputs with the different FC technologies available today [18].

Regenerative fuel cells

The fuel cells presented above convert energy one way: from fuel to electricity. They are not designed for the reverse recharging operation. Recharging the fuel cell requires an electrolyser (EZ) to decompose the water back into hydrogen and oxygen. The electrolyser is generally a separate unit from the fuel stack and the two cannot operate simultaneously. The coupling of a FC stack and an EZ stack is conventionally known as Regenerative Fuel Cell (RFC). With an electrical energy efficiency for the electrolyser of 90% and that of the fuel cell of 60%, the overall round trip efficiency of the systems will be about 54%. The life is estimated to be 10000 hrs.

In high power applications, mass optimized RFC units may provide up to 1000 Wh/kg. The specific energy, however, is sensitive to various thermal and electrical design requirements [17].

Unitized regenerative fuel cells

The Unitized Regenerative Fuel Cell (URFC), also known as reversible PEM fuel cell, or reversible regenerative fuel cells, refines this concept by using the same cell electrodes to perform both the electrolyzer function and the fuel cell function. The system is based on PEM cells, and uses bi-functional electrodes. No system performance or efficiency is lost compared to either fuel cells or electrolyzers constructed in this reversible geometry [17].

Electrolizer

Before ending this chapter, let's have a brief introduction about this technology.

The electrolysis process is the inverse of the fuel cell one, and has been developed before and in parallel with fuel cell technologies. In the area of space missions, few electrolyzers were developed for some particular usage, as in the case of the water electrolyzers used in the ISS to produce breathing oxygen for the crewmembers.

The two main electrolyzers technologies developed until now are the alkaline and PEM electrolyzers. Alkaline electrolyzers were commercially and widely used but the PEM one is growing, despite the higher cost (noble metal catalysts) [17].

2 Fuel cell test rig reconfiguration

This Chapter describes from the very beginning of the assignment, the entire test bench reconditioning process. After the introduction briefing at Polytechnic of Turin, is started a preparation phase on multidisciplinary studied based on F.Iannicelli's thesis [17]. The acquired knowledge were essential to start the seven months internship period at EAC, working at direct contact with the FC test rig.

2.1 Background

Iannicelli's thesis work is based on modelling and simulation of SAPS to create a first proof-of-concepts tool to support future similar systems design, which should be able to cope with the harsh lunar environment and to supply energy demand of both the base and crew.

The SAPS elements are managed by a control logic, which select the right operation according to the actual power request and the production rates. The model merges all the main and most relevant aspects involved in SAPS operations, as also transient phenomena. The simulations have been based onto a mission scenario, which demonstrate the system capability to work with different conditions of power request and mission duration. This thesis work, starts from this point and is targeting the model validation through a test campaign using a FC test rig.

2.2 Initial project goals

1. Integrate the new stack in the old test rig;
2. Validate the MATLAB/Simulink model (polarization curve);
3. Power part of LUNA, FLEXHab, and/or MARVIN rover.

The experimental phase is focused on the FC, especially on the integration of the FC new stack into the old test rig. Since the stack is quite delicate and expensive, it was necessary to partially redesign the subsystems and test them, as well as electronics set-up. The FC is automatically regulated by the control electronics, which control the cooling system and the air compressor, whereas the power electronics manages the main power output.

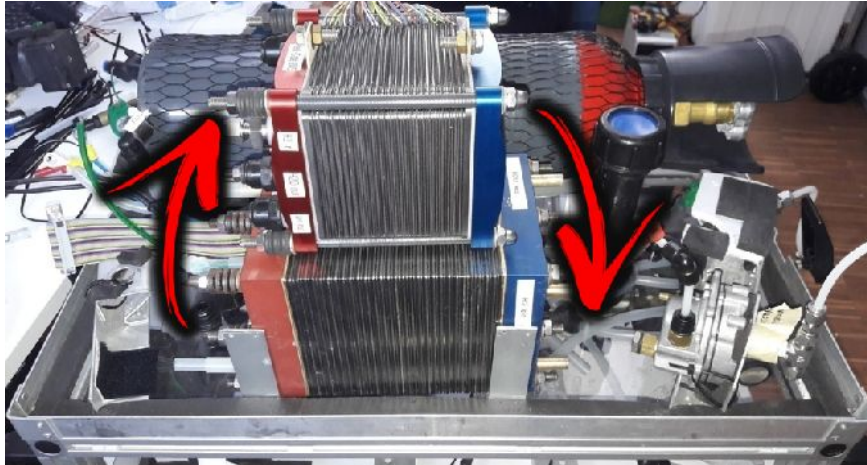


Figure 22. New stack (top), old stack (bottom).

The test campaign aims to provide the FC polarization curve for validating the simulations. In this way, it is possible to optimize and create a robust simulation environment for accurate performance predictions in order to have accurate predictions even for different stacks, sub-systems and configurations, thus reducing futures experimental costs.

Nevertheless, before proceeding with the model validation, the Simulink model (Figure 23) has to be modified for accounting the changes with respect to the old FC test rig:

- Update the hydrogen circuit;
- Create a preheating circuit;
- Integrate the necessities improvement at the existing model blocks:
 - Correct the humidity model.
 - Create a cooling subsystem.

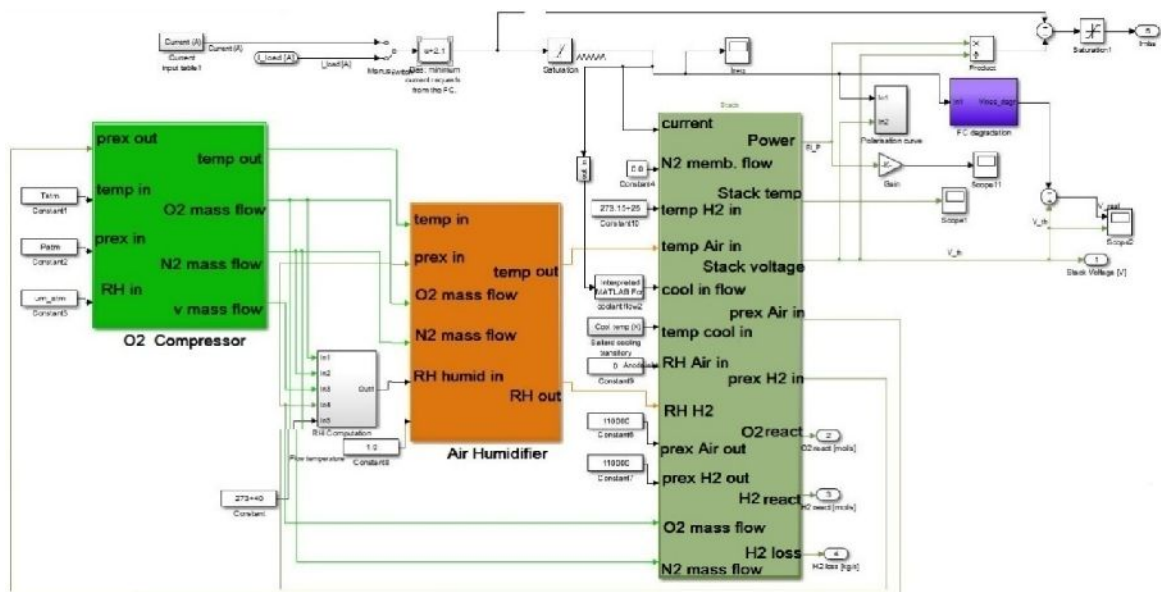


Figure 23. FC SimuLink scheme

Once the FC will be in perfect operative conditions, it would be used to power a part of LUNA and, FLEXHab (*Figure 24*), to do experiment inside them, or to recharge MARVIN (*Figure 25*) batteries.



Figure 24. LUNA rendering



Figure 25. Rover MARVIN

For the reason that will be explained, the whole thesis is spent on the stack integration.

2.3 Old test rig configuration and new stack

The FC power bench was designed and installed as an Auxiliary Power Unit (APU) for an experimental hybrid ultralight aircraft. It was able to produce 500 W and weights 32 kg (8.5 kg of FC stack). The FC was a PEM type produced by ZSW[©], model name BZ100-30 (30 cells).



Figure 26. Old test rig configuration

That stack has been substituted with BZ100-13 (24 cells), also from ZSW[®], which has 1 kW of nominal power, i.e. double the power, half the weight and dimensions, thus, four times the electrical density, of the old one. Between the two stacks, there are about ten years of differences and technology improvements. For this reason, they have quite different features, as the need to redesign the H₂ circuit and a more powerful water pump.

The old stack has been substituted to increase the power output and for its damages (hole in the membrane).

It can be noticed that a certain level of separation between the test rig upper part (hydrogen “part”) and the lower part (contains electronics and a brushed motor) exists to reduce as much as possible the risks of hydrogen ignitions in case of leakages or malfunction.

2.4 First contact with FC test rig

The first contact with the test rig was not optimal due to:

- Storage conditions;
- Lack of datasheets and information regarding the electronics and subsystems components;

The new FC stack was found with unsealed connectors (*Figure 27*): letting the air and thus poisoning gas as CO₂ to degrade the internal membrane, in particular, impairing a bit the rare metals responsible of the catalyst function.

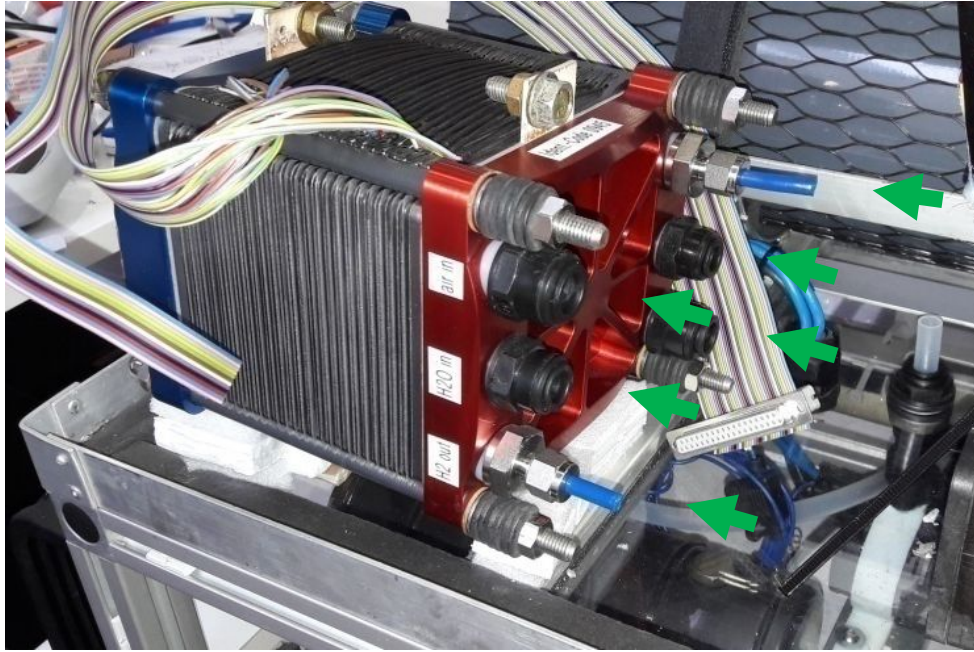


Figure 27. Unsealed stack arrows indicate the unsealed in/output

To verify the compatibility of old subsystems with the new stack requirements, it was fundamental to know their data and parameters; unfortunately there was a completely lack of any datasheets and a partial documentation of the FC stack too. For some components, it was possible to retrieve the documentation thanks to the serial number and model printed on them, however, for the others, an experimental characterization was necessary (paragraph 2.9 *Components characterization*).

A focus has to be done on the control and power electronics were ad-hoc developed for APU, with a pre-load fixed working point, (quite far from the freedom of test rig concept), without documentation too. All this consideration leaded us to discard the electronics and design a new one.

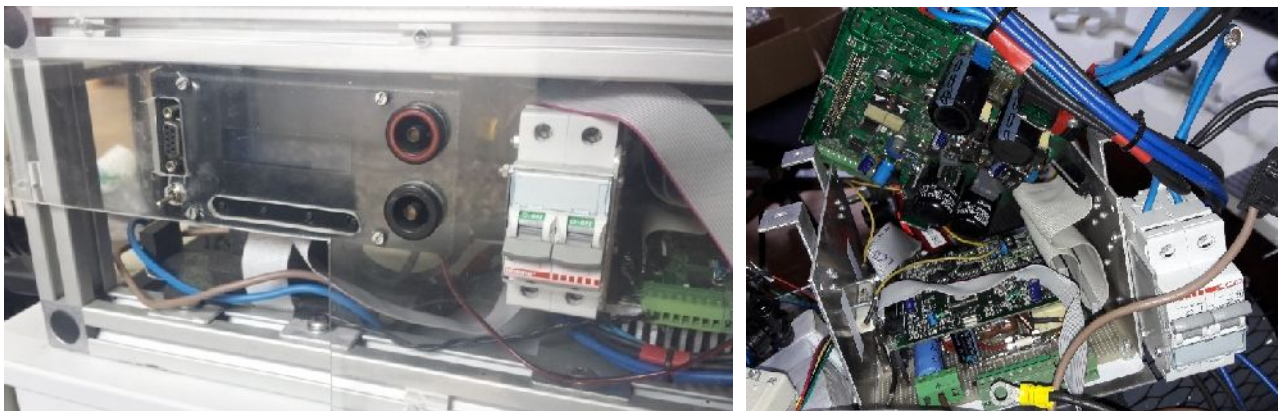


Figure 28. Old electronics

2.5 Action plan

The first two months of the internship were spent in components datasheets searching, specifically with Dr. Joachim Scholta (from ZSW[®]) for FC stack data, and stack integration within the test rig. In particular, a new part of the H₂ subsystem has been designed, defining how to sense all the subsystems, and a draft configuration of the overall test rig has been designed.

2.6 Fluid circuits

Essentially there are:

- two gas circuits: Air (with water vapor too) and H₂
- water circuit as cooling

2.6.1 Air circuit

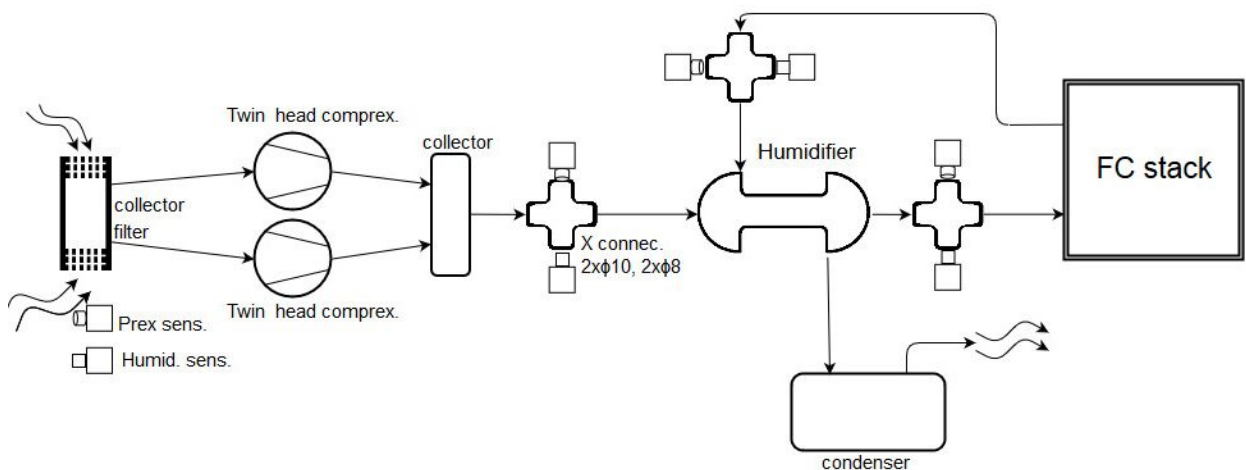


Figure 29. Air circuit scheme

The FC is air breathing, so it means that takes O₂ from air. The control (by the control logic) of this subsystem is important because the FC output power mainly depend from it.

The key element of the circuit is the passive humidifier. This element is quite simple because it does not require any external (logic) control and electric power. On the other hand, this component imposes a longer start-up transient and slow working variation.

The air, after being compressed by the membrane compressors, enters inside the humidifier where receives heat and water vapour. The FC chemical process is exothermic: the majority of the oxygen reacts with hydrogen, becoming water, so partially absorbing the heat produced via evaporation. Therefore, at the cathode output there is hot air (~ 60°C) poor in oxygen and reach of water vapour (a small amount of liquid water is also present). This flow

enters inside the humidifier exchanging heat and humidity through the membrane with the air that will enter inside the FC. Finally, air (cooled down and with a lower humidity level) goes into the condenser before exiting the circuit.

2.6.2 Cooling system

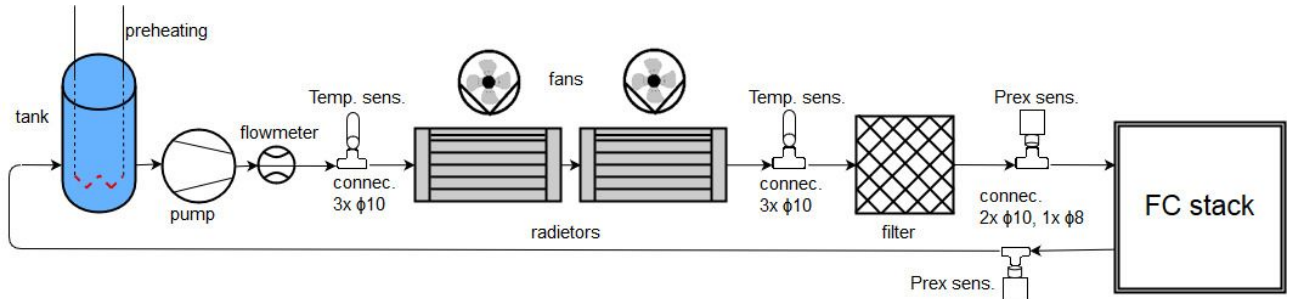


Figure 30. Cooling circuit scheme

The cooling system is quite simple. It is composed by a water-cooling and a preheating system. The preheating system will be located inside the water tank. Since it was developed in the last week of internship, it was simply made by a car light bulb (light efficiency <3%, thus heat efficiency >97% !!).

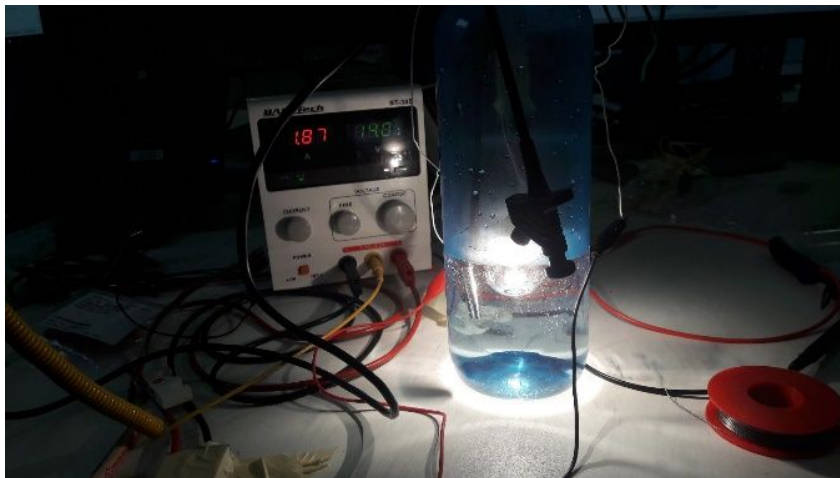


Figure 31. Preheating test

2.6.3 Hydrogen circuit

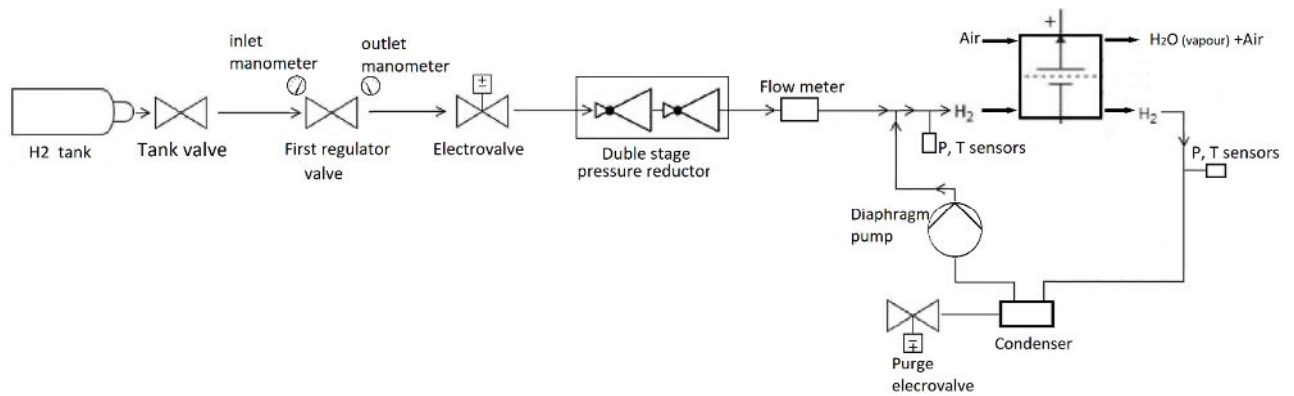


Figure 32. Hydrogen circuit scheme

The H₂ circuit is the most critical one due to the intrinsic H₂ explosiveness (easy sparks ignition) and for the FC sensibility at this gas (a starvation of this gas causes irreversible performance decay). This circuit was redesigned to avoid the stack flooding, adding sensors, 3D printed supports, and a recirculation pump.

The first two valves are manual, and are used to reduce the tank pressure (200-300 bar) to 2-5 bar. The electrovalve is used simply as shut-off valve controlled from the control electronics (see paragraph 2.7 *Control logic*). The most important valve is the dual stage valve (DSV), it precisely reduces the upstream pressure (not constant) to the FC feeding pressure (constant at 1.2 bar).

The new stack requires a permanent H₂ flow during operations, different from the old one that had a “dead-end” anodic circuit. Since the required flow is major than the reactant rate, it is mandatory to create a recirculation of the not-reacted H₂. In order to gain the load losses inside the stack, a H₂ recycling pump, brushless to avoid any spark risk in “the hydrogen floor”. It was chosen to buy a twin head diaphragm pump (Teflon membrane against H₂ degradation) and use only one head for the H₂ recirculation and the other for the rig ventilation, instead of a very expensive custom pump. It has to be noticed that sloping stack output circuit is necessary to collect the water in the condenser tank and to be expelled through the purge valve.

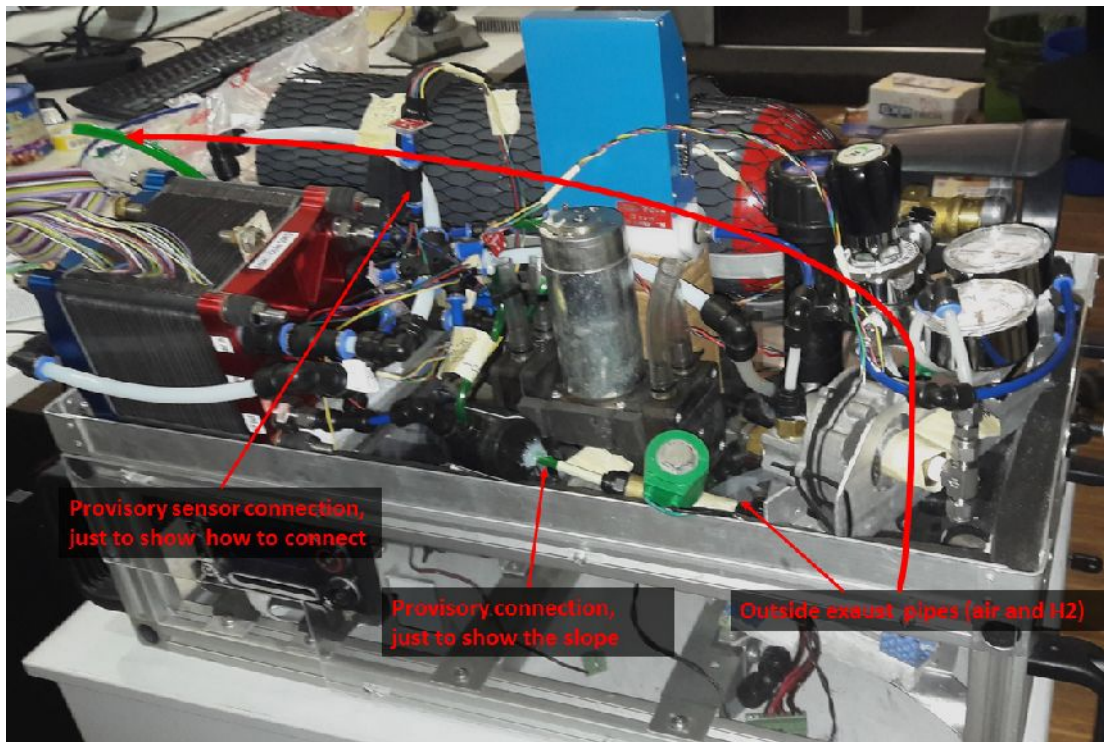


Figure 33. Provisory assembly side view

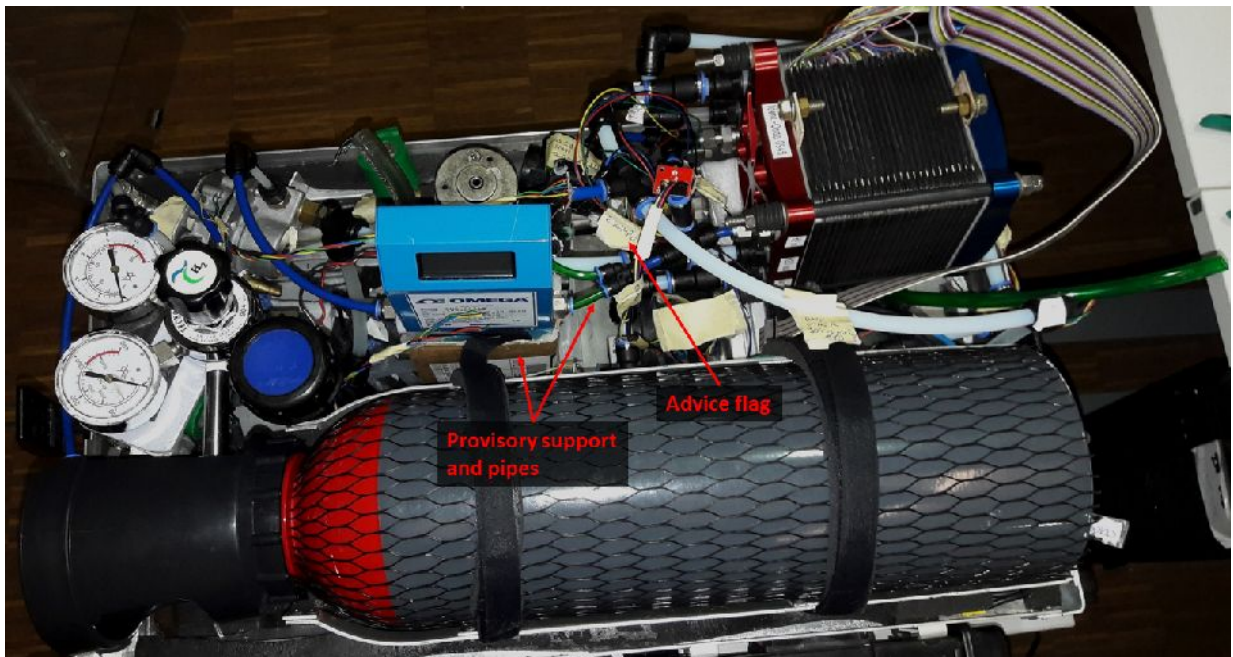


Figure 34. Provisory assembly up view

2.7 Control logic

The electric circuit is the other main subsystem of the test rig. It controls the test rig operations and power distribution. It can be divided in control electronics and power electronics.

The FC is usually coupled with auxiliary batteries to absorb power fluctuations required from the external load. Since the FC has quite slow dynamic, a fast power logic is needed to avert the under-voltage which causes irreversible performance decay. The power logic was not taken into account during the internship, because the external (electronic) load is always known, stable and regulated, at least in the testing e validation phases.

Regarding the control electronics, before choosing the hardware components and designing all the connections, it is necessary to create the logic flow (*Figure 35*) to merge the test rig operation needs and the FC constrains.

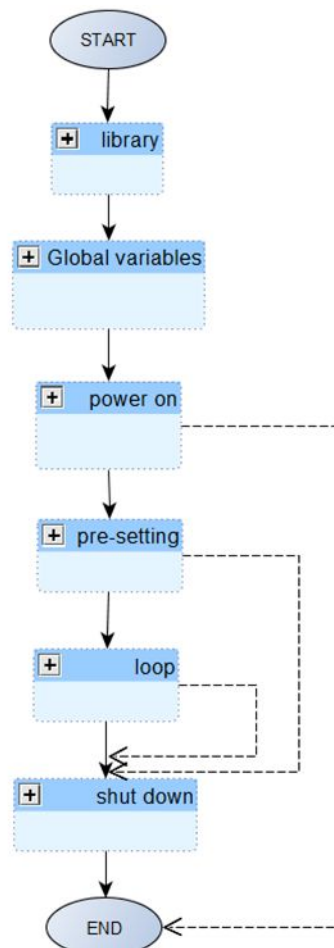


Figure 35 Flow diagram

Errore. L'origine riferimento non è stata trovata. Inside each block there are other sub-blocks containing sub-flow with series of specific actions, which have to be executed from the test rig components (*Figure 36*).

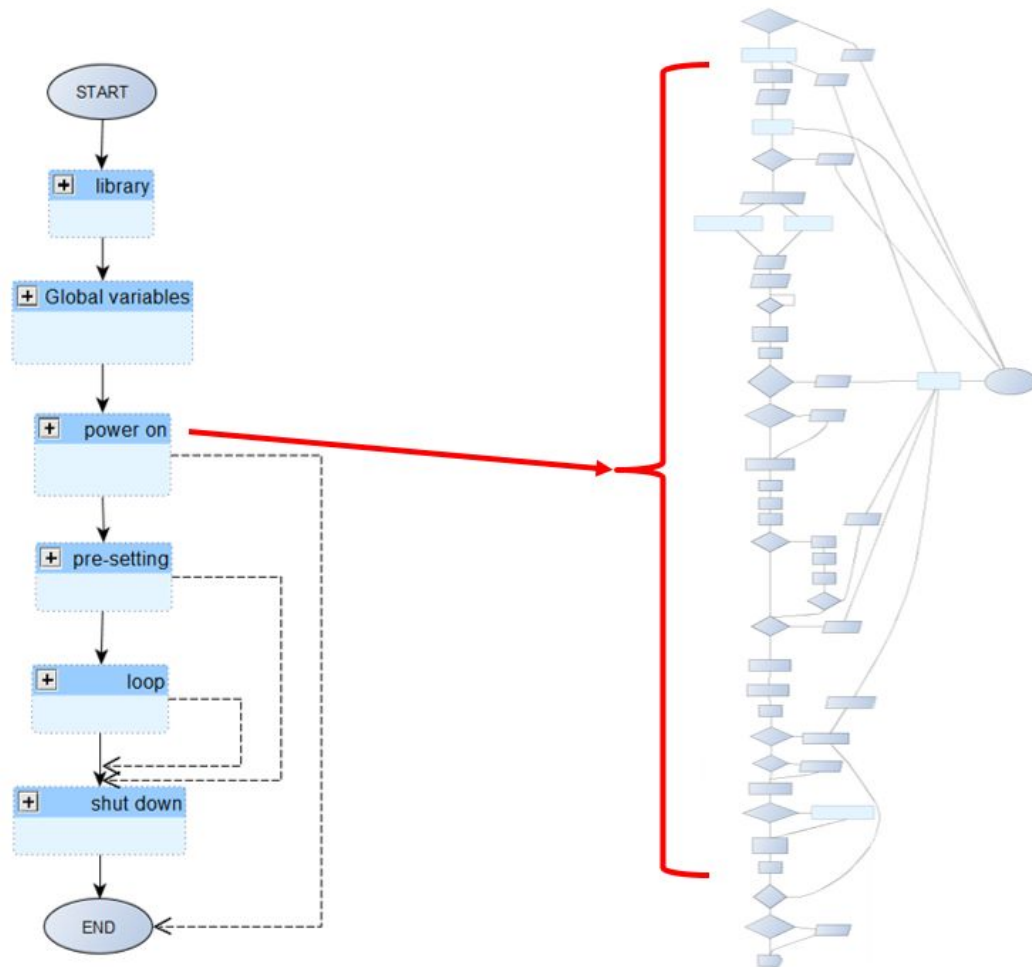


Figure 36. Sub flow chart

The control logic flow chart has been detailed enough to ensure its direct transposition into a programming language. For example, *Figure 37* shows a rhombus which compares two pressures, so to be then written as an “if” statement, regardless the language syntax adopted.

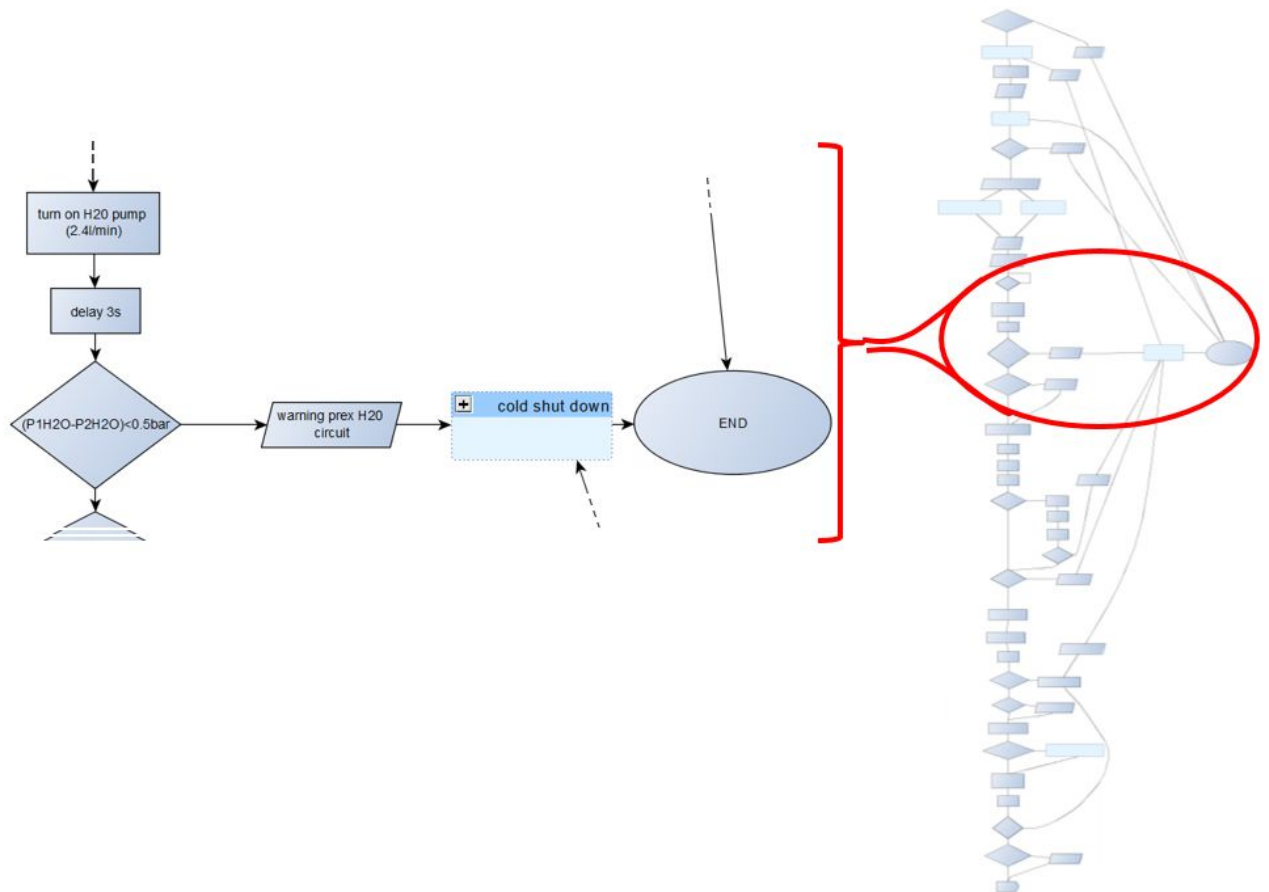


Figure 37. Flow chart detail

2.7.1 Power-on block

Only the critical alarms are active in this block. When the operator turns on the “master switch” (Figure 38.1), the electronics is powered and the program execution begins. In the power-on block, there are all the initial checks (sensors and environment conditions), preheating and subsystems tests necessary for proper FC operations. Afterwards, the operator has to choose one of the operation modes, connect the load, and turn on the “start operations switch” (Figure 38.2). The operation modes are the following:

- *Normal operation mode*: the test rig is automatically set at the optimum working condition (960 W, 14.4 V, 66.7 A)
- *Setup mode*: to be used by experienced users only
 - Manual regulation: in this mode it is possible to set a starting point and change some setting values (air flow, cooling temperature, purge time etc.) during the test;
 - Automatic regulation - PC monitoring: in this mode it is possible to upload a load profile, visualize it, and record all the test rig sensors data. To be used for the Simulink® model validation;

- Brake-in: this mode should be used for the stack brake-in procedures, which have to be used at every first test rig power-on after 6 inoperative months.



Figure 38. Master switch (1) and start operations switch (2)

2.7.2 Pre-setting block

In this block, all the values and the necessary actions are computed to ensure the right steady operation regime by all the subsystem. At the end of this procedures, all alarms and monitoring sensors are activated.

2.7.3 Loop block

In this block, the instructions are executed in a loop. There are all the sensors monitoring and components feedback control, such as:

- H₂ pump loop;
- Air pump loop;
- Purge valve loop;
- Voltage control loop;
- Electronics temperature loop;
- H₂ leak detector;
- Humidity monitoring;
- Gas pressure control loop;
- H₂O pressure control loop;
- Temperature loop;
- H₂O pump loop.

From this block onwards, the power is supplied to the load with continuous operations.

2.7.4 Shut down

In this block, there are all the automatic and manual (operator duty) operations for a proper shutdown. This block is activated into three different ways:

- End of the chosen operation;
- Switch off the “operations switch” (*Figure 38.2*);
- Emergency shutdown due to an out of range value (in this case the shutdown procedure is not the standard one, to avoid stack damage).

2.8 Net architecture

A key factor considered while developing the control logic was the hardware architecture and how to split the various routine in different parts. Complexity, accuracy, and cost were the main design drivers considered to choose among different solutions. Specifically, the final architecture chosen is sketched in *Figure 39*.

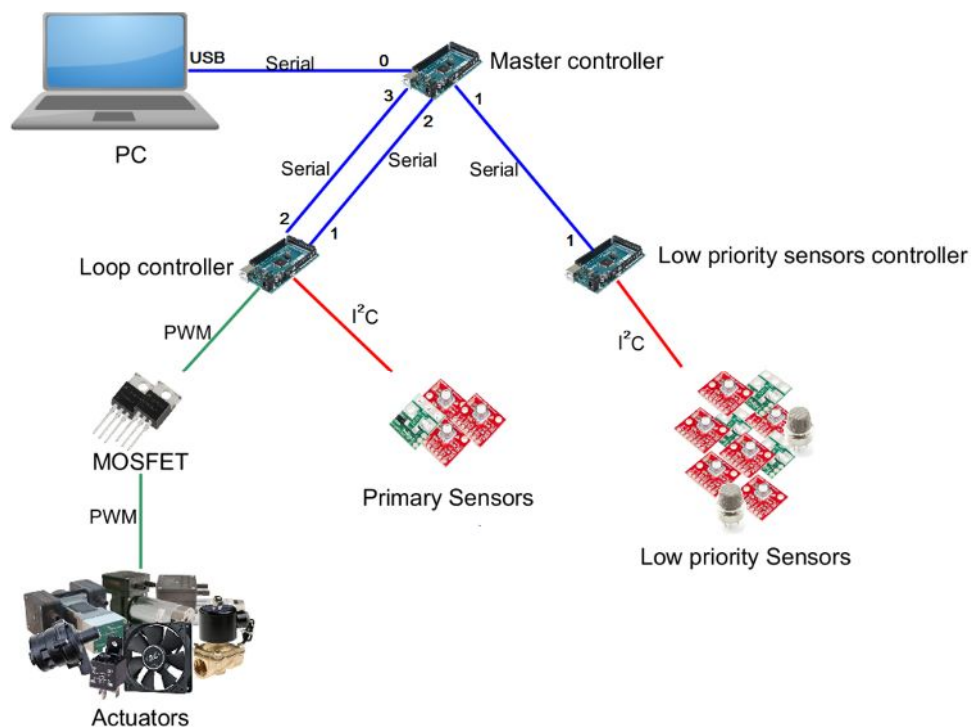


Figure 39. Net architecture

2.8.1 PC

The PC was used to visualize all the sensors data, to give commands, and to eventually adjust parameters, using the master control. The Master Control (MC) is the processor selected for managing all data in input from the sensors and in output to the actuators accordingly to the control logic. The MC also establishes the communication between processor and computer. The computer is connected with the master controller by a serial protocol (serial channel 0 -

USB). Visual Basic has been used as software interface. Several intermediate scripts have been done to achieve the ultimate interface version using the Vb.NET language. Each Visual Basic script works only with the proper Arduino script, so it is important pay attention on the files titles, since them univocally links the scripts. In *Figure 40* it is possible to see the interface of the “*Test_10_Graph_Trackbar.sln*” script: it has been used to implement and verify the trackbar command while the chosen values are showed and recorded. The interface pattern reported in *Figure 40* is the default ones and until the program in not running the graph are showed as bar graph. Indeed commands to customize the graph are inside the code in order to easily set up the same options for all the programs. Once the debugging starts, graphs automatically became line graphs and values are displayed as function of time. The communication between the master controller Arduino and the computer is based on a single serial channel. Hence to avoid overlap in the communication, values are firstly read from Visual Basic, then processed (information are showed in graphs and text boxes, and saved in a .txt file), and finally commands are sent back to the MC Arduino. The time for this continuous loop depends on the amount of data to manage, because the Arduino processor (bottleneck) needs time to elaborate all information. Therefore, the pause time between one loop and the other one should be set accordingly to the intrinsic time cycle of Arduino, adding then circa 30 ms for safety purposes.

It was payed attention to comment every script line to lead an easier updating for future development.



Figure 40. Graphical interface in Vb.NET. Default interface pattern while the program is not running

2.8.2 Master controller

For the Master controller (MC) it is possible to use a single-board computer (RaspberryPI) or a micro controller (Arduino). RaspberryPI would be a good choice (faster and multi thread processing) but because several Arduino Mega were already present, and for their ensured compatibility with all sensors, they were chosen as the final devices to use. The master controller executes the main flow logic, instruction by instruction. In addition, it can take decisions relying on data coming from the controller loop (serial channel 3) and can send commands (serial channel 2) to actuators through the same controller loop. The MC does not execute a loop but a linear flow and it has to exchange data with all the serial channels with variable time period. Therefore, every time that a peripheral has to communicate with the MC, it has to generate an “interrupt” for pausing the MC main instruction, execute a sub-routine (exchanges data and execute eventual actions), and finally continue with the MC instruction flow. The best way to do this is with an “attachInterrupt” which use a digital pin to activate a specific interrupt.

The code was written as a unique program, instead of many isolated micro controller programs, for a correct programming architecture. Conversely, this choose, brings with it the necessity to divide the code in the micro controllers. Inside the folder contains all the control logic, there are two extension file type:

- the “.h” containing the script dedicated to a specific micro controller (ex. “main_MasterControl.h”) or a repetitive action (ex. “SerialProtocol.h”) ;
- “.cpp” (ex. “*main.cpp*”) distributes the write function inside the write controller.

Below is described as example the procedure to compiles the code inside the MC.

The MC script has to be written inside “*main_MasterControl.h*”. To compile all the software in the Arduino micro controller, the entire folder containing the control logic has to be copied inside the folder of micro controller , and the “*ControlLogic>main.cpp*” file has to be copied inside the Arduino’s workspace, making sure to uncomment only the line relative to that micro controller. Finally, execute the Arduino’s workspace. *Figure 41* shows the MC Arduino’s workspace scenario.

2.8.4 Low priority sensors controller

This controller simply reads the sensors value and sends (serial channel 1) them to the PC one every two seconds.

2.9 Components characterization

The experimental characterization is necessary for all the components whose datasheets were missing and for those critical for the test rig operations, which have to be finely tuned. Precise regulation is also required for the subsystems with no feedback sensors installed, i.e. the output is known from the characterization curve without any live operational feedback. An example is represented by the air compressors flow regulation, since there is not an air flow meter.

The characterization was necessary for the following equipment:

- H₂ flow meter;
- H₂O flow meter;
- Dual stage valve;
- Air compressor;
- H₂O pump;
- Arduino;
- Voltage sensor.

Most of the characterization procedures include the intrinsic Arduino read error, since it was noticed and corrected with a characterization too, only at the end. So, only the Voltage sensor characterization is not influenced by Arduino's error (corrected in separated way).

2.9.1 H₂ flow meter

This was the first characterization; it was quite simple, assuming as the value read from the instrument display as the real one. Those values were compared with the proportion between the output data signals and the full scale of the instrument.

The error of this method ranges between 0.2 lpm (for low flows) and 1 lpm (for high flows). Therefore, a finer tuning was necessary: the error was computed for different flow speed, to

minimize it. The correction equation obtained is $F = F_a * 1.011 + 0.12$, where F is the real flow and F_a the flow reads from Arduino.

After the all characterization campaign, we noticed that this error was directly correlated to Arduino and not to the instrument itself, as reported before.

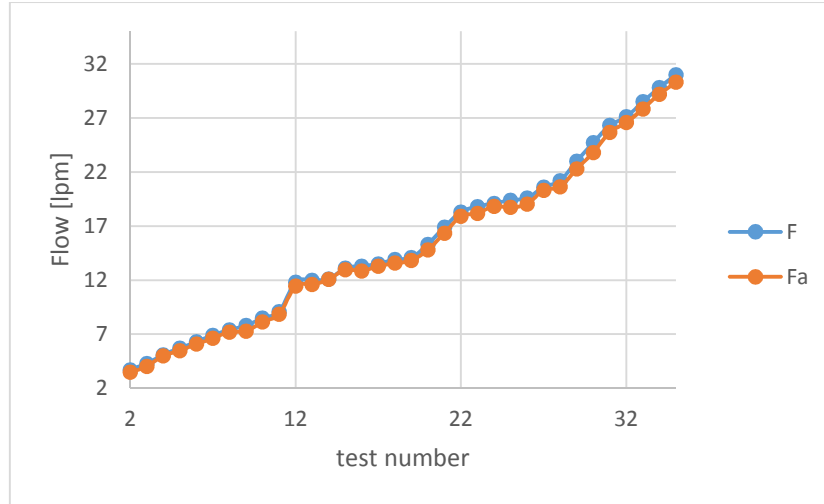


Figure 42. Differences between the measured and real flow

2.9.2 H₂O flow meter

This section describe how to find its conversion constant. The sensor working principia is detailed in section

2.10 Sensors2.10 Sensors. Starting from the datasheet formula, a correction was made to calculate the calibration constant, after different flow speed tests. An indirect method was used to calculate the (mean) flow, i.e. it was derived by measuring the time to fill a certain

water volume. This approximation can be considered precise since the measurements were executed under specific operative conditions:

- Precise volume and time measurement instruments (milligrams balance and milliseconds chronometer);
- Sample time longer than operator reflex (human mean response time = 200 ms, so if the test runs over 10 s, the error will be under 2 %).



Figure 43. Water flow meter test set-up

It was quite tricky to find this constant since it has an exponentiation influence on the final flow value. Hence to avoid to use the try and error approach, we have made only four runs and after insight the power behavior, we made an extrapolation to find the constant value that would give the smallest error between the direct measure (flow meter) and the indirect one was then performed (Figure 44).

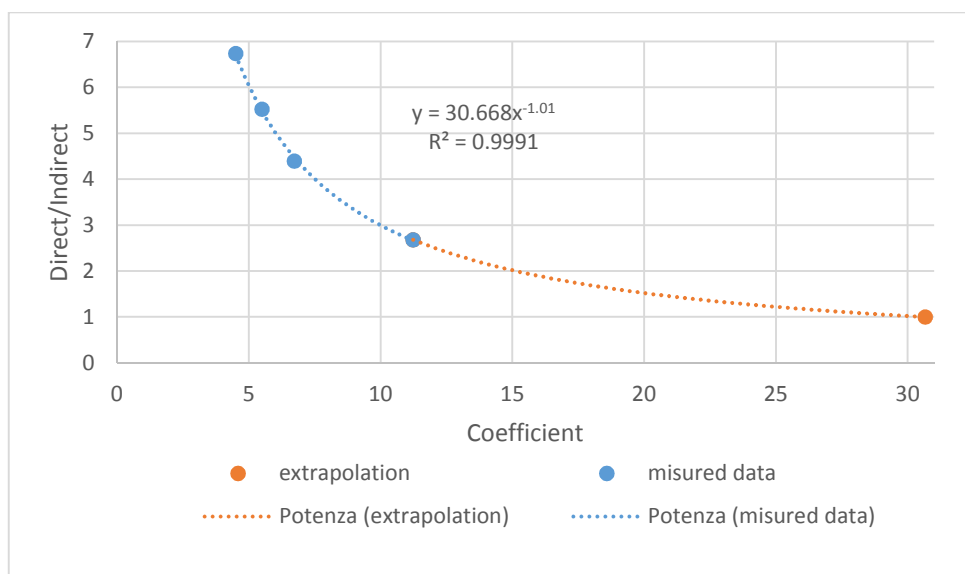


Figure 44. Coefficient extrapolation graph

In conclusion, the error has been estimated to be under 5 %, a quite good result considering that was achieved without a precise value of the water flow.

2.9.3 Dual stage valve

For this test, it was verified that the DSV could had guaranteed the values of pressure and flow required by the FC stack. Different tests were performed, changing the upstream pressure (from an external compressor) and the exhaust valve position. To simulate the FC load losses, air was flowing inside the old stack.

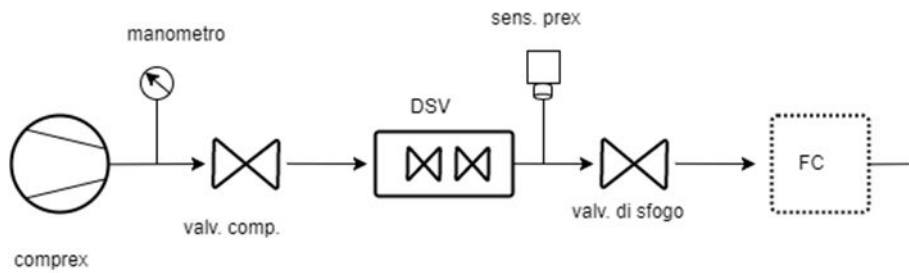


Figure 45. DSV tests experimental scheme

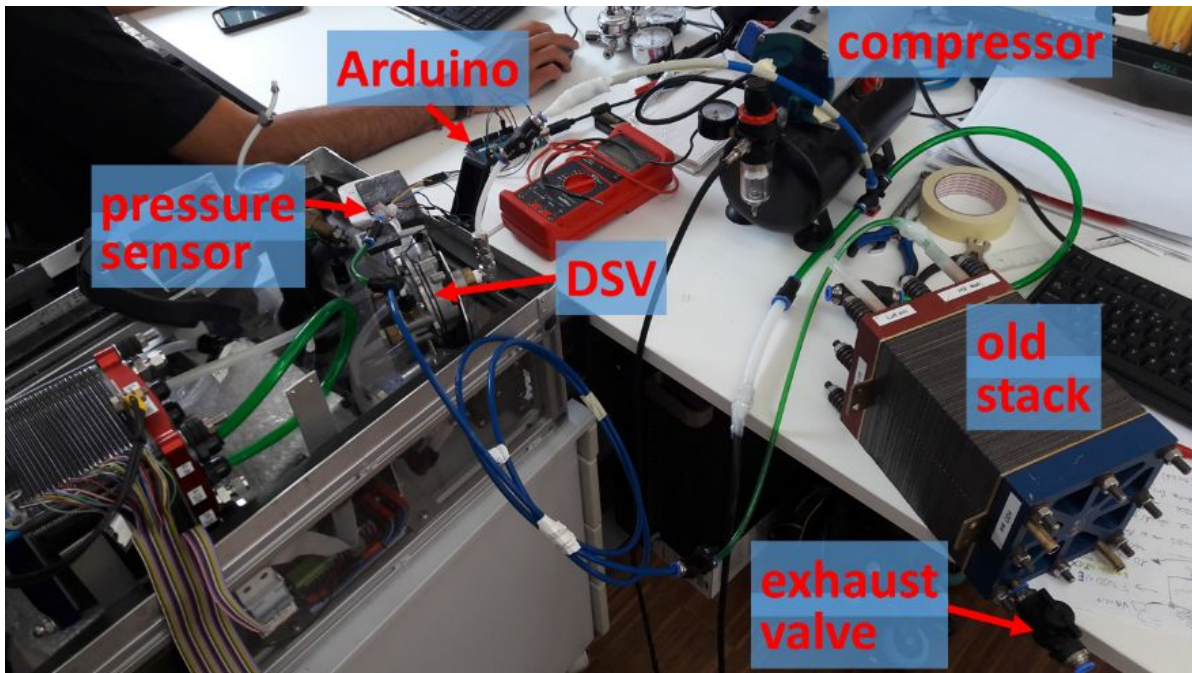


Figure 46. Experimental setup

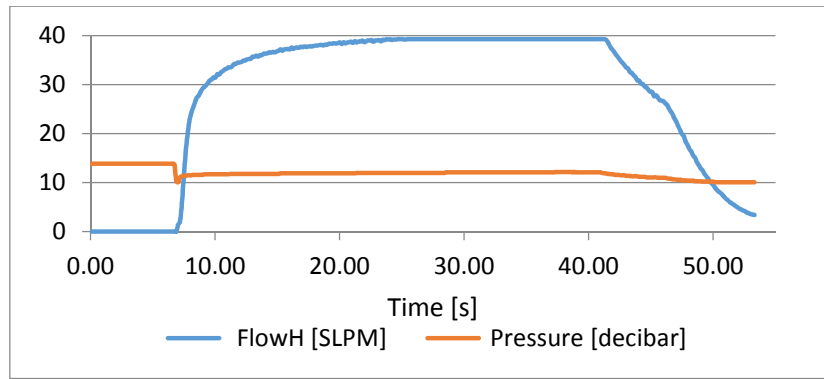


Figure 47. Flow - Pressure characterization curve

The actual flow was over to 40 lpm, (the H₂ flowmeter could not measure up to that value) more than stack constrain. The experimental setup scheme (Figure 45) is slightly different from the one shown in Figure 46, but they work in the same way.

2.9.4 Air compressor

The membrane compressor is quite important to properly perform an experimental characterization, due to the lack of feedback flow sensors.

We have borrowed the H₂ flowmeter, pressure (after the compressor), flow, voltage, and current were measured for 11 tests runs. The physical quantities varied were:

- The voltage supply (thus the compressor speed), to simulate operating different flow requests;
- The exhaust valve position to simulate the load losses due to the FC stack (Figure 48).

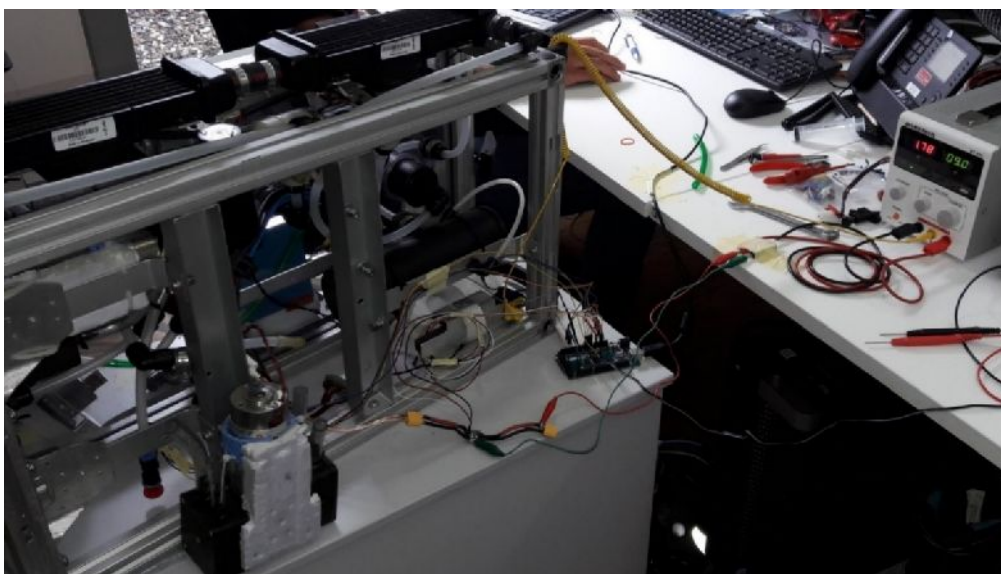


Figure 48. Air pump characterization

It can be noticed that the compressor portrayed in *Figure 48* is not the one used for the test, in fact it is not connected.

After the test campaign, the first thing to do before using the data is to adjust them in a usable form. We have noticed an annoying fluctuation in the data (*Figure 49*) and they are principally related to:

- The data acquisition system itself, i.e. not physical variations;
- Actual oscillations of the membrane pump.

Since only the mean value oscillations were of interest, a custom-made noise-reduction algorithm has been used to diminish as much as possible the fluctuations without altering the real behaviour of the system (*Figure 50*).

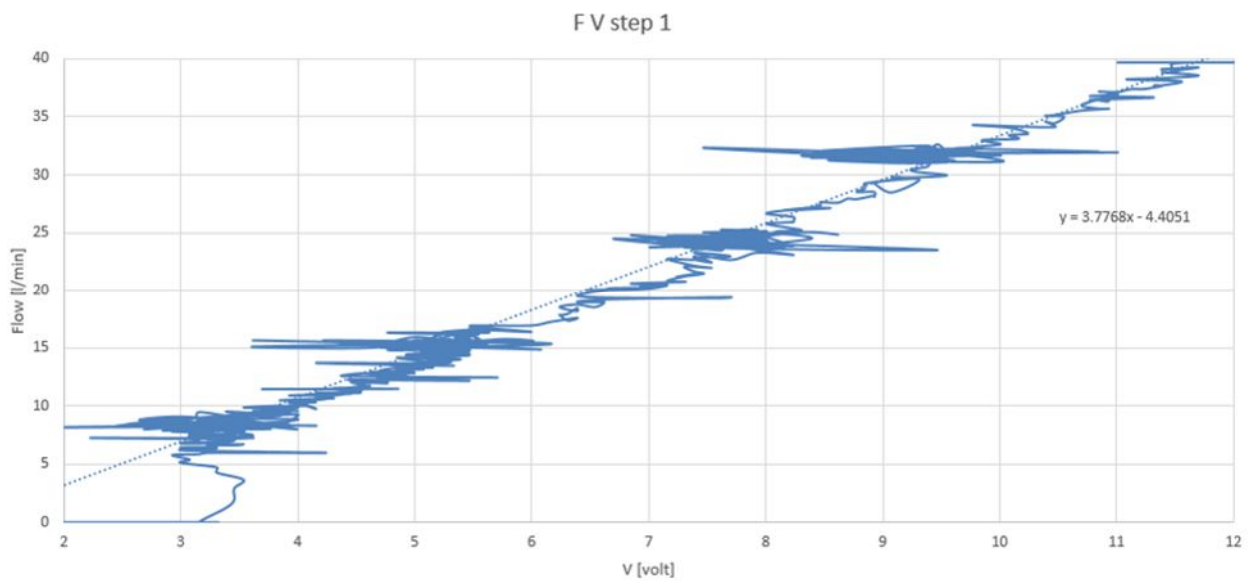


Figure 49 Original data

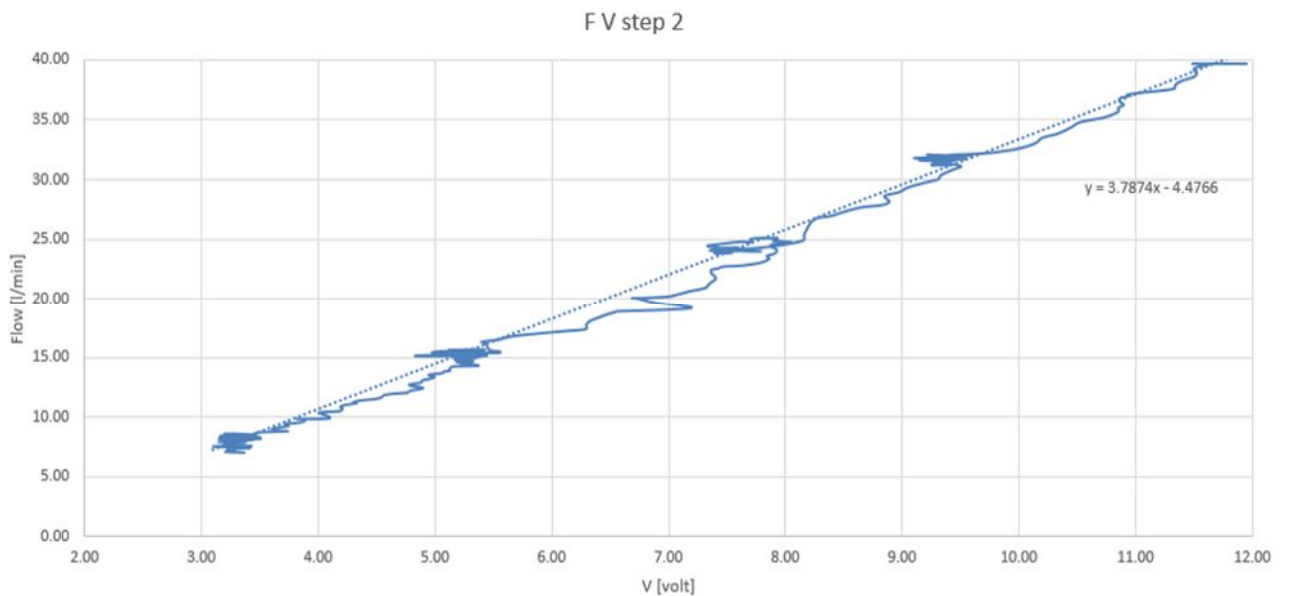


Figure 50 Noise reduced data

The next step was to create a characterization equation that can link pressure, flow and voltage. This was quite hard due to the non-linear behaviour of them, so a semi-empirical interpolation equation has been adopted. Results are reported in a excel automatic calculation table where just voltage and pressure values are needed to calculate the flow (of one compressor).

2.9.5 H₂O pump

This component suffered from some trouble before the characterization task. It worked for some minutes (in the trial setup) but “died” shortly afterwards. After disassembling and testing all the hydraulic and electrical components, a burned fuse was found in the electronic board. A new fuse was installed to start the characterization procedure.

The characterization has been done twice, since the old (repaired) pump did not give enough flow, so a new one was bought.

The experimental setup is quite similar to the air compressor one. The water flows through all the cooling system components at exception of the stack. Pressure (after the filter), flow, voltage and current were measured during several test runs. The voltage was constant inside each run but was changed between one test and the others (*Figure 51*).



Figure 51. Water pump test set

From the experimental data it was extrapolated the flow-voltage curve and so the equation (linear behaviour).

Regarding to the new pump, the characterization analysis was not done since from the very first dry run the flow was not enough for our purpose. The problem regarding the second pump will be explain in the section 2.13 *Unexpected challenges*.

2.9.6 Arduino

The Arduino characterization was not hard, but very critical for the whole test rig operations, which are based on the indirect Arduino measurements. The analogue read ports have been simply powered with a tension between 0 and 5 V (controlled with high precision Voltmeter) and compare with the Arduino read one. Arduino does not read directly the input volt, but displays it as an interval from 0 to 1023 (16 bits float), so it should be converted into V via multiplying it by a factor of $5/1023$. This method is not so precise, so a semi-empirical characterization procedure was necessary.

From the first graph (Figure 52), it can be noticed that the lowest readable value is not 0 but about 0.08V and the maximum one is 4.66V. From the second graph (Figure 53), a great improvement after the characterization can be noticed, which reduces the error to almost zero for the majority of the values within the range.

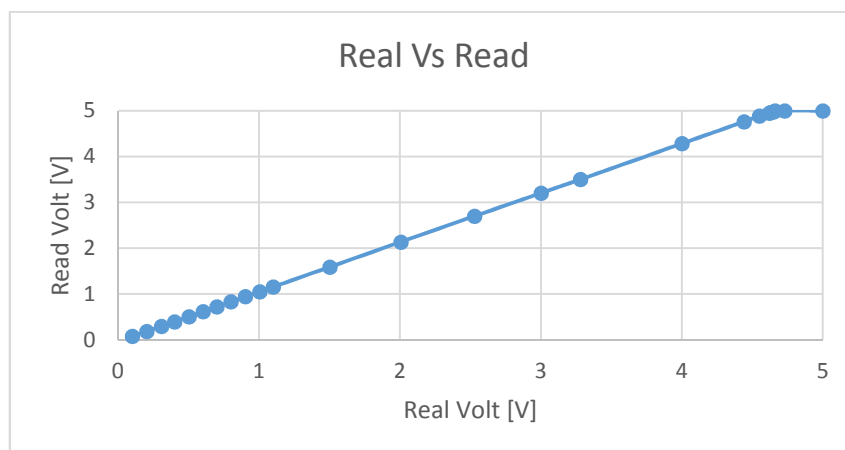


Figure 52. Value comparison

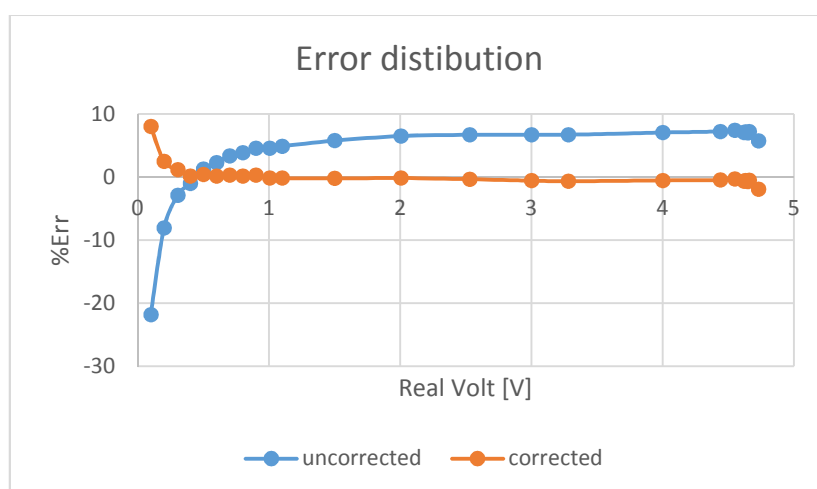


Figure 53. Error distribution

In this way, it is possible to directly convert the “*analogueRead*” (i.e. the levels between 0 and 1023) into voltage values using this equation $V = 0.0045 * analogueRead + 0.036$ (it may be different for another Arduino). In other characterizations (the volt sensor for example), the Arduino analogue read level has been directly converted into the desired physical quantity, without using the voltage. Therefore, an indirect measurement less, that leads to have more precise conversion with less error propagation.

2.9.7 Voltage sensor

As the Arduino, this sensor is critical for the indirect measurements and all components control without feedback. The same procedure used with Arduino on the 45A and 180A sensors type has been adopted. The best fit of the experimental data is a perfect linear equation, even if quite different from the manufacturer datasheet one; indeed, the new correlation reduces the error from about 10 to almost 0 % .

It has been found that the voltage sensor is responsible of a non-negligible voltage drop. Therefore, the characterization was made using the sensor out-voltage as reference, and not the in-voltage, to be sure of the voltage that the downstream components will receive, is the same measured. It would be good to do a characterization of the sensors voltage drop as well, related at the in-voltage.

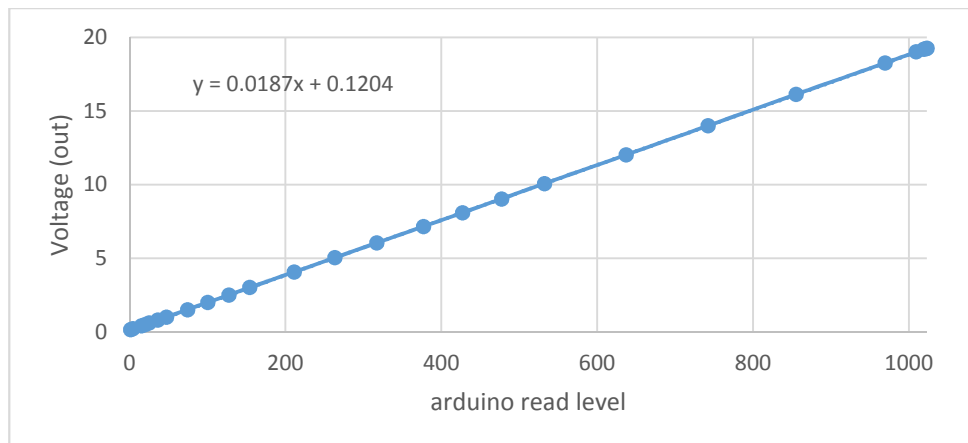


Figure 54. Voltage sensor (45A) characterization chart

It can be noticed that this voltage sensor associated with Arduino cannot achieve the nominal performances declared from the manufacturer .

voltage sensor type	nominal max voltage	actual max voltage
A45	13.6 V	19.25V
A180	50 V	73.2V

Table 6. Features of voltage sensors

Those values correspond at the Arduino analogue read saturation (1023).

As final note, these sensors should measure the current too, nonetheless they do not work.

They have unexpected behaviors not suitable for the application of the FC test rig (Figure 55).

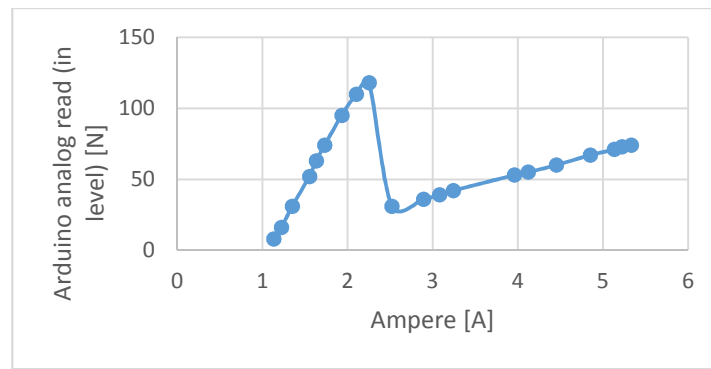


Figure 55. Attempt of current characterization (45 A type)

In Figure 55, it can be noticed the piecewise linear behaviour. An hypothesis could be that it is broken, however the most probable cause is the scale limit to 45 A (in Figure 55), which is too big to measure currents under 3 A, where it has not a linear behaviour; this fact is add to the Arduino bad behaviour under the analogue read level 150.

2.10 Sensors

To measure all the critical parameters for the FC model validation, the following sensors have been selected:

- 12x pressure and temperature;
- 4x humidity and temperature;
- 1x flowmeter H₂;
- 2x flowmeter H₂O;
- 2x voltage and current;
- 3x temperature;
- 3x hydrogen gas detector (safety reasons).

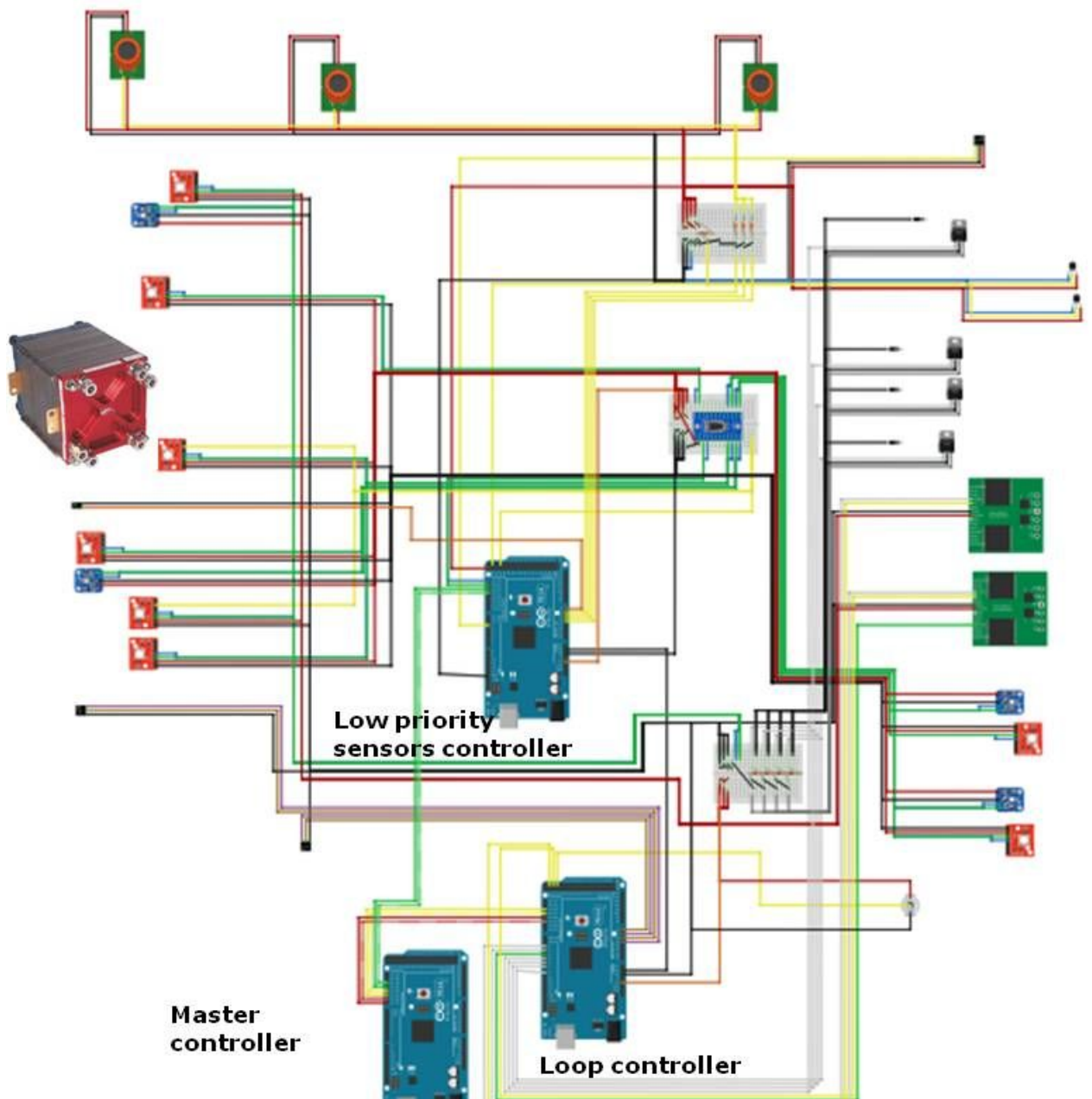


Figure 56. Sensor circuit

It could be possible that some connections amount components of the hydrogen circuit have a gas leakage and in this case it is important to reveal leakage and promptly act. The chosen sensors are both analogue and digital. The analogue sensors are connected individually to the Arduino analogue pins to avoid communication overlaps or errors are avoided. It is possible to use as many sensors as the number of available analogue pin. The digital sensors (pressure and temperature, and humidity and temperature) use the communication protocol Inter Integrated Circuit (I^2C): it is based only on two specific wires, one for Serial Data (SDA) and a second one for Clock Signal (SCL), enabling communication amount one controller (called master) and several sensors (called slaves) on a single communication bus.

The advantage of using the I²C protocol is the ability to exchange information more sensors at once with only two master ports. On the other hand, this protocol has a speed reduction strictly related to the number of slaves and the number of identical sensors that can be used in the same I²C bus, which is as well limited to the number of different addresses available to the sensor. These two problems especially affects the pressure and temperature sensor since it has only two addresses and just one I²C bus is present in the Arduino MEGA. The workaround used is the I²C Multiplexer TCA9548A even if this causes an additional communication delay.

Considering all the communication problems and the speed required to control the key parameters of the FC stack, it has been decided to divide sensors in two groups according to the required refresh rate. To avoid stack under tension, the vital sensors to monitor the key parameters of the FC have been set as “primary sensors”, i.e. at the maximum possible communication speed. All the other sensors have been grouped as “low priority sensors” since their values can be checked less frequently; as already explained in *2.8 Net architecture* paragraph.

In *Figure 56* it is possible to see the physical circuit scheme that reflects the simplified schematization in *Figure 39*. The scheme represents all the sensors and actuators, and how

they are connected one another. The wiring logic is also important: each color refers to a specific signal, as reported in [Table 7. Relation wire color - signal](#)

Color	Signal
Black	Ground
Red	+3.3 V
Orange	+3.3 V from controller to breadboard
Green	Serial Data (SDA)
Blue	Serial Clock (SCL)
Yellow	HIGH/LOW Signal
White	PWM Signal
Grey	Ground for MOSFET
Ochre	Voltage information from C&V sensors
Purple	Current information from C&V sensors

Table 7. Relation wire color - signal

Two exceptions are present, due to the already existing wires of the components:

H₂ Flowmeter → Orange: data signal;

H₂O Flowmeter → Red: + 5 V;

H₂O Flowmeter → Yellow: data signal.

From the central breadboard of the scheme it is easy to recognize the I²C Multiplexer and, from that, the low priority sensors controller. The remaining sensors and all the actuators are connected to the controller loop, which is the one with a high number of PWM pins. The last Arduino in the scheme is the Master control that is only connected to the microprocessors and to the PC. This scheme depicts not only real connections but also their position in the test bench. The components on the left side of the Master controller are indeed placed at the top level of the test bench, where the hydrogen circuit is present and electronic components are minimized for safety reasons. All the other components placed in the right side, including

the controllers, are located at the bottom level of the bench, creating a safe separation from hydrogen.

The electronic boards connected to a heatsink and a fan. This assembly solution is ideal to have low temperatures nearby the microprocessors.

When the wiring of the circuit scheme will be completed and sensors will be assembled into the fluids circuits, it is suggested to proceed with sensors potting. This process, with the selected epoxy potting compound, provides a protection against water and hydrogen wear. The special epoxy resin is suited for electronic components since it is able to remove heat from "hot spots" while not affecting the temperature sensors.

2.11 Actuator supply

Arduino has an imitated output power, sufficient for electronics components, but poor for power actuator operations. It was designed two power busses for the actuators power supply (24 and 12V), and use Arduino analogic (PWM) or digital pins as control signal. This is true only for the brushless twin head H₂ pump, while for the other actuators require an intermediate component to rise even the Arduino voltage signal. It was used a transistor (type Ultrafast Speed IGBT, 100 A) to convert the PWM signal (used for fans and water pump) and a relay for the digital one (for the electrovalves). Finally, the two air brush compressors are driven from an integrated dual "H bridge" model: Pololu Dual MC33926 Motor Driver.

2.12 Graphic interface communication

In order to perform the components characterization and to manage the information acquired by sensors and actuators during FC operations, a graphical interface is needed. Since in the hardware architecture is not yet present a screen and a mass storage, the use of a computer is necessary to visualize real time the key parameters and save them.

Two different solutions could be implemented. One is to code all commands using a computer software (e.g. LabVIEW) and the Arduinos only as data acquisition (DAQ) boards. Alternatively, a second strategy is to program Arduino micro-controllers to work autonomously and using a computer software as graphical interface. Of course, both strategies have pros and cons. Using an external software as LabVIEW provides a fully suite for data managing: visualize, command, and store. Indeed, all data are elaborated from the computer processor and no more from the Arduino's micro processor. Hence computing time is minimized and graphical capability is maximized, because the computational power provided by a computer is way more than the one provided by the Arduino's micro processor. This first solution requires a deeper knowledge of the engineering software and a longer developing time. Then it has been chosen the second solution, where a graphical user

interface has been developed using the Visualbasic.NET programming language (Vb.NET). The PC is only used to visualize values from sensors and possibly to give commands. This solution is based on the processing unit of the micro controller (where all the code is written) and on a single serial connection. Of course, the computational power is limited, but developing new parts of the code and improving them is easier thanks to the huge Arduino online community. Moreover, the code has been written only once and can work independently with a computer. Instead of using the Arduino's serial monitor, it has been preferred to develop a graphic interface in a more powerful environment as Visual Basic, which can also create stand-alone applications.

The logic behind the scripts is the similarity between Arduino and Visual Basic codes. There is a first part where some libraries are imported and all global variables are defined as string, integer, boolean, vector, or datatable. Then, with the subroutine "*Form1_Load*", communication with Arduinos and the data storage is set. Some other sub-functions are created for visualizing data with the desired design. Here it is possible to define all parameters related to graph and save the same diagrams features for every run. The sub-function "*Timer1_Tick*" reflects the "*void loop()*" Arduino function. The instructions wrote in this sub-function are continuously repeated: each loop firstly reads what the Arduino Master Control sent with the function

$$data = SerialPort1.ReadLine()$$

where all the Arduino outputs are stored in the string *data*. The subsequent command

$$dataPt = data.Split(",")$$

distinguishes in the string *data* all the information that are separated with a "," and store them in the vector of strings "*dataPt*". At this point it is possible to work with all values, make calculations, and assign them to charts. Now it is also possible, using the Arduino environment, to send information through the serial port with the instruction

$$SerialPort1.Write(TrackBar1.Value + 1 & ";")$$

where inside brackets it is directly given the value of the track bar number 1 as integer. This is the simplest case, because only one value is given. Adding new values is however really easy. It is only a matter of adding "&" before the value and "&," after it. In this way, the instruction "*SerialPort*" creates a unique string of values separated from semicolon. It is interesting to note the "+1" added to value inside brackets, because it is part of a security check in the data transmission. This little add allows the code to reduce bugs in case of

dysfunctions and increase its robustness. It is also worth to mention that information sent from Arduino are separated with a coma and the ones sent from the graphic interface are separated with a semicolon. Anyway, Arduino is able to recognize the strings and separate values into single variables with the instruction

Serial.parseInt()

that has to be repeated as many times as the number of values sent from the graphic interface. Thanks to this convection for data transmission, it has been possible to standardize all scripts, giving commands at the same time of reading values between micro controllers and the graphic interface.

2.13 Unexpected challenges

During the internship period several unexpected challenges have been faced which had required more work than the original planning.

The first challenge arose when looking for datasheets of all the test rig components. This easy task resulted into a long series of investigations and calls since some components had no part number or the customer support was no able to find proper documentation about them. For example, the water pump and the had no part number on its. While for DSV, the manufacturer had no more references because it has been made as unique component and no more documents were found in the archive. Because of this problem, it has been decided to characterize the water pump and the DSV.

Later on, during the net architecture definition, we dealt with the communication protocol of the pressure and temperature sensor breakout. The manufacturer of this sensor claimed that was able to communicate using two protocols, i.e. I²C and SPI, as confirmed by the related datasheet. After having analysed which protocol would have performed better for the FC application, SPI was chosen. This protocol uses a master-slave architecture with a single master. The master device originates the frame for reading and writing. Multiple slave devices are supported through selection with individual slave select (SS) lines. Sometimes SPI is called a four-wire serial bus, contrasting with two-, and one-wire serial buses. Then, in comparison with the I²C protocol, communication with SPI protocol results in higher throughputs and simpler hardware interfaces. However, the manufacturer did not verified how the SPI protocol effectively works for that sensor. The technical customer service suggested us to try with a bi-directional logic level converter in order to step down 5V signals to 3.3V. Unfortunately even this suggestion did not resolve the problem.

The technical customer service guided us in all tries and at the end it also gave up promising a future feature check. Therefore, we decided to switch to the I²C protocol that is far slower than the SPI and it need a multiplexer for more sensors with the same address on the bus. The presence of a I²C multiplexer introduced a new unexpected challenge: it was the primary problem which led to avoid the use of LabVIEW as sensors reader. Almost one month has been spent for code analysis and developing but it was not possible to include the multiplexer between Arduino and sensors, so to manage information with LabVIEW. The main reason is due to a special LINX library created from the LabVIEW community to increase the use of Arduino. LINX library allows a medium-level user of LabVIEW to connect devices and applications while taking advantage of built-in algorithms for data manipulation, controls, and mathematical analysis [6]. On the other hand, LINX library has to be used as a “black box” and the built-in functions are not easily changeable. Consequently, when a special sequence of instructions for the I²C multiplexer was needed, the LINX library could not include it, so everything have been restarted from scratch with Visual Basic. The system runs slower and less smoothly compared to LabVIEW, but was easier to develop.

ELEKTRISCHE WASSERPUMPE BOOSTER EBP15 12V DAVIES CRAIG

Förderleistung: 15,0 l/min. bei 0,1 bar

Temperaturbereich: -40°C bis 120°C

Stromversorgung: 9V-15V Gleichstrom

Stromaufnahme: max. 1,3 A

Anschluss: 19mm

Platzdruck: 2,5 Bar

Figure 57. Futures of the ordered Electric water pump

Beside the above-mentioned difficulties, there were some hardware related issues. During the water pump characterization, it suddenly stops to work. At a first glance, there was nothing different and as well as no burning smell. On account of this, the pump was disassembled and an electronic board fuse was found blown. A new one was used as replacement and the pump was repaired in just one week. Unfortunately, at the end of the characterization, the maximum flow measured was not sufficient for the FC stack. The new FC stack requires a minimum flow of 4,8 l/min and the pump could provide a maximum of 2 l/min. With this result, a new pump was needed. Considering automotive water pumps, which were in line with the bench requirements, a specialized online shop for racing car

spare parts was chosen as supplier. *Figure 57* reports the features of the selected water pump, in line with the FC requirements. Sadly, the measured maximum flow was 4 l/min instead of the 15 l/min reported. This value was measured in a pre-test configuration, where load losses were less than 0.1 bar. This low water flow value could irretrievably damage the FC stack.

Additionally, for the hydrogen recirculation circuit, a brushless pump was needed. Even if the pump was ordered in August, it has not been delivered yet (last update: end of October, with an estimated arrival date of mid-November).

In conclusion, many problems were faced: examination, solutions searching, and trials took a considerable amount of time. Some of them were solved, but some others (time constraints or manufacturer support) still prevented the FC test rig to start.

3 Future steps

For future interns, the work should be resumed from the final packaging and storage showed in *Figure 58*. The FC test rig is in a prototype configuration with temporary brackets and guide labels to provide the vision of how the final set-up should look like.



Figure 58. Final packaging and storage

Therefore, to reach the fully operational capabilities of the FC test bench, these are the required steps:

- Install the hydrogen pump for recirculation in the hydrogen circuit.
Wait for the pump delivery (mid-November), as mentioned in chapter 2.13 Unexpected challenges, replace it with the brushed air compressor positioned in the upper level, and connect all the missing parts for completing the hydrogen circuit.
- Find a new solution for the water pump.
The previously bought pump could give only 30% of the datasheet Values. One solution is to use two H₂O pump in a parallel configuration to reach the minimum water flow

required, or buy a new and more powerful one. The last solution is of course the better one, but requires a market survey;

- Design and develop the power electronic.

Application of solid-state electronics to the control and conversion of electric power, managing the FC power output. For example, it is important to monitor the load power request for peaks absorption with backup batteries.

- Sensors and control breadboards potting to protect themselves from wear (harsh environment related to water and hydrogen) and dust.

Wires fixing and electric circuit consolidation are paramount to have a safe and reliable test environment.

- Complete the control logic code with sub-functions for sensors and alarms loops.

These codes partially exist, but only the main structure is done. The emergency stop procedure has been developed but not yet coded: it is then desirable to include it into the control logic.

- Developing graphics and command interface for external users through Visual Basic.

This is essential for testing the test bench, characterizing the FC stack, and for standalone operations. The basic commands have been already developed, but further improvements are more than welcome. A user interface for the embedded system is desirable, possibly using the previous LCD screen.

Of course, all those steps are believed to fulfill the primary goal of the project, i.e. FC start-up and testing. Unexpected challenges still might happen, but following the above-mentioned points will lead to complete the system for obtaining the experimental polarization curve and finally validating the lumped parameters model.

4 Conclusions

The fuel cell (FC) technology has not gained a great diffusion yet, but its trend is absolutely positive. Many companies are operating in the FC field, creating new applications thanks to more powerful and efficient solutions. The FC test rig project is in fact intended to analyze and verify a new FC system for future space application.

Starting from the reconversion of the old test rig for the new stack, more than hundreds of new parts and components have been selected and bought. The most challenging part was the sensors choice due to the specific range of humidity, pressure, and temperature to cover. The very first approach to the FC stack was only with its operational manual, whose data were insufficient to cover all the open points. The FC stack was stored for a long time with unsealed cups, which resulted into a mandatory recondition. Besides to this fact, the entire test bench had to be adapted for the new FC stack. Thanks to several talks with the FC manufacturer, it was possible to acquire the necessary knowledge to work with this delicate equipment. FCs are generally sensitive to changes, and they can modify their response with tenths of seconds. Therefore, it is decisive to analyze and interpret the FC's parameters, in order to program automatisms for counter-reacting in time. Hence, the procedures for reconditioning, setting, and the control logic have been written carefully. Moreover, before using the FC stack, hydrogen, air, and cooling water should be managed in a proper way. At the beginning of the internship there were no information for some components and a characterization was necessary for the following: air compressor, dual stage valve, H₂O pump, H₂O flow meter, voltage and current sensor and Arduino. Then instead of using ad hoc components, Commercial Off-The-Shelf (COTS) ones were adapted for the FC application, which requires high speed and parallel control. The developed hardware and software architecture has been used for all characterizations, providing a successful application. Most of FC parameters could be controlled separately thanks to both hardware and software. In fact, to control the oxygen, water, and hydrogen flows, as well to generate energy, it is mandatory to individually regulate all pumps, fans, and relays. The current version of the software is already able to run specific tests, such as reading, visualizing, and saving all the required values. All these operations are the bases of future FC test bench

applications. For example, for training purposes, it could be useful to have a total control of the parameters to finely tune each of them.

In conclusion, when the hydrogen pump will be delivered and a plausible solution for the water pump will be found, all the fluid circuits could be completed and integrated to supply the new FC stack.

This thesis study closes the first loop designed. Surely, the work accomplished can be improved and optimized in the following loops.

Bibliography

- [1] D. Massey, *The Vision for Space Exploration*, 2004.
- [2] I. S. E. C. G. (ISECG), "The Global Exploration Roadmap" 2018.
- [3] D. Smitherman, "Deep Space Habitats," no. II, 2015
- [4] M. a. R. a. S. Thompson, M. a Rucker and S. Thompson, "Developing a habitat for long duration, deep space, pp. 1–10, 2012.
- [5] C. Careri, *Preliminary design and modelling of a photovoltaic plant for a crewed lunar outpost*, 2017.
- [6] P. G. e. al., "Illumination conditions at the lunar south pole using high resolution digital terrain models from lola Icarus", vol. 243, pp. 78–90, 2014.
- [7] P. D. Spudis, *Physical environment of the lunar south pole from clementine data: J. Chem. Inf. Model.*, vol. 53, no. 9, 2013.
- [8] D. A. P. e. al, "The lunar reconnaissance orbiter diviner lunar radiometer experiment," pp. *Space Sci. Rev.*, vol. 150, no. 1–4, pp. 125–160, 2010.
- [9] D. A. P. e. al, "Diviner Lunar Radiometer Observations of Cold Traps in the Moon's South Polar Region,," pp. *Science (80-.)*, vol. 330, no. 6003, pp. 479–482, 2010.
- [10] A. E. M. Casini, "A Virtual Reality approach for studying a future human lunar outpost: an integrated simulation case study of a Stand Alone Power System," *68th International Astronautical Congress (IAC), Adelaide, Australia, 25-29 September 2017. IAC-17.A3.2C.10*.
- [11] D. A. Smith, "Space Launch System," no. November, 2016.
- [12] M. a. R. a. S. Thompson, "Developing a habitat for long duration, deep space missions," *Glob. Explor. Conf*, p. pp. 1–10, 2012.
- [13] E. S. Agency. [Online]. Available: http://www.esa.int/About_Us/EAC/European_researchers_invited_to_board_Spacehi. [Accessed 2018 03].
- [14] S. S. Loral, "International Space Station," pp. vol. 24, pp. 69–75, 1998.
- [15] B. Company, "International Space Station Electric Power System," p. pp. 1–23, 2011.

- [16] Spectrolab, "XTJ Prime datasheet," 28th July 2016.
- [17] F. Iannicelli, "Modelling, simulation and experimentation of a regenerative energetic system for space applications," 2016.
- [18] E. Testa, "Multidisciplinary design and optimization of innovative electrical power systems for aerospace applications," 2013.
- [19] Greenbuilding. [Online]. Available: <http://www.rinnovabili.it/greenbuilding/case-off-grid-thailandia-piu-grande-sistema-solare-idrogeno-222/>.
- [20] [Online]. Available: <https://www.intechopen.com/books/nanocomposites-with-unique-properties-and-applications-in-medicine-and-industry/a-review-of-thermoplastic-composites-for-bipolar-plate-materials-in-pem-fuel-cells>. [Accessed 14 03 2018].
- [21] D. A. Larminie J., "Fuel Cell System Explained," 2002.
- [22] I. EG&G Technical services, "Fuel Cell Handbook," 2004.